
ELEMENTARY PARTICLES AND FIELDS
Theory

**Near-Threshold Production of $a_0(980)$ Mesons in πN
and NN Collisions and a_0-f_0 Mixing***

**L. A. Kondratyuk, E. L. Bratkovskaya¹⁾, V. Yu. Grishina²⁾,
M. Büscher³⁾, W. Cassing⁴⁾, and H. Ströher³⁾**

*Institute of Theoretical and Experimental Physics,
Bol'shaya Cheremushkinskaya ul. 25, Moscow, 117259 Russia*

Received April 8, 2002

Abstract—We consider near-threshold $a_0(980)$ -meson production in πN and NN collisions. An effective Lagrangian approach with one-pion exchange is applied to analyze different contributions to the cross section for different isospin channels. The Reggeon exchange mechanism is also evaluated for comparison. The results from πN reactions are used to calculate the contribution of the a_0 meson to the cross sections and invariant $K\bar{K}$ mass distributions of the reactions $pp \rightarrow pnK^+\bar{K}^0$ and $pp \rightarrow ppK^+K^-$. It is found that the experimental observation of a_0^+ mesons in the reaction $pp \rightarrow pnK^+\bar{K}^0$ is much more promising than the observation of a_0^0 mesons in the reaction $pp \rightarrow ppK^+K^-$. Effects of isospin violation in the reactions $pN \rightarrow da_0$, $pd \rightarrow {}^3\text{He}({}^3\text{H})a_0$, and $dd \rightarrow {}^4\text{He}a_0$, which are induced by $a_0(980)-f_0(980)$ mixing, are also analyzed. © 2003 MAIK “Nauka/Interperiodica”.

1. INTRODUCTION

The structure of the lightest scalar mesons $a_0(980)$ and $f_0(980)$ is still under discussion (see, e.g., [1–7] and references therein). Different authors interpreted them as unitarized $q\bar{q}$ states, as four-quark cryptoexotic states, as $K\bar{K}$ molecules, or even as vacuum scalars (Gribov’s minions). Although it has been possible to describe them as ordinary $q\bar{q}$ states (see [8–10]), other options cannot be ruled out up to now. Another problem is the possible strong mixing between the uncharged $a_0(980)$ and the $f_0(980)$ due to a common coupling to $K\bar{K}$ intermediate states [11–17]. This effect can influence the structure of the uncharged component of the $a_0(980)$ - and implies that it is important to perform a comparative study of a_0^0 and a_0^+ (or a_0^-). There is no doubt that new data on a_0^0 and $a_0^+(a_0^-)$ production in πN and NN reactions are quite important to shed new light on the a_0 structure and the dynamics of its production.

In our recent paper [18], we have considered a_0 production in the reaction $\pi N \rightarrow a_0 N$ near the threshold and at GeV energies. An effective Lagrangian approach and the Regge pole model were applied to investigate different contributions to the cross section of the reaction $\pi N \rightarrow a_0 N$. In [19], we have employed the latter results for an analysis of a_0 production in NN collisions. Furthermore, in [17], we have considered the a_0-f_0 mixing in reactions involving the lightest nuclei d , ${}^3\text{H}$, ${}^3\text{He}$, and ${}^4\text{He}$. Here, we give an overview of those results and present a comparative analysis of $a_0(980)$ -resonance production and nonresonant background channels in the reactions $\pi N \rightarrow a_0 N \rightarrow K\bar{K}N$ and $NN \rightarrow a_0 NN \rightarrow K\bar{K}NN$. Our study is particularly relevant to the current experimental program at COSY (Jülich) [20–22].

Our paper is organized as follows. In Section 2, we discuss the $K\bar{K}$ and $\pi\eta$ decay channels of the $a_0(980)$. An analysis of $a_0(980)$ -resonance production and nonresonant background in the reactions $\pi N \rightarrow K\bar{K}N$ and $NN \rightarrow a_0 NN \rightarrow K\bar{K}NN$ is presented in Section 3. Section 4 is devoted to the calculation of the cross sections for the reactions $NN \rightarrow NN a_0$ and $NN \rightarrow a_0 NN \rightarrow K\bar{K}NN$ in comparison to nonresonant $K\bar{K}$ production. In Section 5, we consider $a_0(980)-f_0(980)$ mixing and isospin violation in the reactions $pN \rightarrow da_0$, $pd \rightarrow {}^3\text{He}({}^3\text{H})a_0$, and $dd \rightarrow {}^4\text{He}a_0$.

*This article was submitted by the authors in English.

¹⁾Institut für Theoretische Physik, Universität Frankfurt, Germany.

²⁾Institute for Nuclear Research, Russian Academy of Sciences, pr. Shestidesyatiletiya Oktyabrya 7a, Moscow, 117312 Russia.

³⁾Institut für Kernphysik, Forschungszentrum Jülich, Germany.

⁴⁾Institut für Theoretische Physik, Universität Giessen, Germany.

2. THE $K\bar{K}$ AND $\pi\eta$ DECAY CHANNELS OF THE $a_0(980)$

The $a_0(980)$ invariant mass distribution in the $K\bar{K}$ and $\pi\eta$ modes can be parametrized by the well-known Flatté formula [23] which follows from analyticity and unitarity for the two-channel T matrix.

For example, in the case of the reaction $NN \rightarrow a_0 NN \rightarrow K\bar{K} NN$, the mass distribution of the final $K\bar{K}$ system can be written as a product of the total cross section for a_0 production (with the “running” mass M) in the $NN \rightarrow NN a_0$ reaction and the Flatté mass distribution function

$$\frac{d\sigma_{K\bar{K}}}{dM^2}(s, M) = \sigma_{a_0}(s, M) \quad (1)$$

$$\times C_F \frac{M_R \Gamma_{a_0 K\bar{K}}(M)}{(M^2 - M_R^2)^2 + M_R^2 \Gamma_{\text{tot}}^2(M)}$$

with the total width $\Gamma_{\text{tot}}(M) = \Gamma_{a_0 K\bar{K}}(M) + \Gamma_{a_0 \pi\eta}(M)$. The partial widths

$$\Gamma_{a_0 K\bar{K}}(M) = g_{a_0 K\bar{K}}^2 \frac{q_{K\bar{K}}}{8\pi M^2}, \quad (2)$$

$$\Gamma_{a_0 \pi\eta}(M) = g_{a_0 \pi\eta}^2 \frac{q_{\pi\eta}}{8\pi M^2}$$

are proportional to the decay momenta in the c.m.s. (in case of scalar mesons)

$$q_{K\bar{K}} = \frac{[(M^2 - (m_K + m_{\bar{K}})^2)(M^2 - (m_K - m_{\bar{K}})^2)]^{1/2}}{2M},$$

$$q_{\pi\eta} = \frac{[(M^2 - (m_\pi + m_\eta)^2)(M^2 - (m_\pi - m_\eta)^2)]^{1/2}}{2M}$$

for a meson of mass M decaying to $K\bar{K}$ and $\pi\eta$, respectively. The branching ratios $\text{Br}(a_0 \rightarrow K\bar{K})$ and $\text{Br}(a_0 \rightarrow \pi\eta)$ are given by the integrals of the Flatté distribution over the invariant mass squared $dM^2 = 2M dM$:

$$\text{Br}(a_0 \rightarrow K\bar{K}) \quad (3)$$

$$= \int_{m_K + m_{\bar{K}}}^{\infty} dM \frac{2M C_F M_R \Gamma_{a_0 K\bar{K}}(M)}{(M^2 - M_R^2)^2 + M_R^2 \Gamma_{\text{tot}}^2(M)},$$

$$\text{Br}(a_0 \rightarrow \pi\eta) = \int_{m_K + m_{\bar{K}}}^{\infty} dM \frac{2M C_F M_R \Gamma_{a_0 \pi\eta}(M)}{(M^2 - M_R^2)^2 + M_R^2 \Gamma_{\text{tot}}^2(M)} \quad (4)$$

$$+ \int_{m_\pi + m_\eta}^{m_K + m_{\bar{K}}} dM \frac{2M C_F M_R \Gamma_{a_0 \pi\eta}(M)}{(M^2 - M_R^2 - M_R \Gamma_{a_0 K\bar{K}}(M))^2 + M_R^2 \Gamma_{a_0 \pi\eta}^2(M)}.$$

The parameters C_F , $g_{K\bar{K}}$, and $g_{\pi\eta}$ have to be fixed under the constraint of the unitarity condition

$$\text{Br}(a_0 \rightarrow K\bar{K}) + \text{Br}(a_0 \rightarrow \pi\eta) = 1. \quad (5)$$

Choosing the parameter $\Gamma_0 = \Gamma_{a_0 \pi\eta}(M_R)$ in the interval 50–100 MeV (as given by the PDG [24]), one can fix the coupling $g_{\pi\eta}$ according to (2). In [25], a ratio of branching ratios has been reported,

$$R_{a_0(980)} = \frac{\text{Br}(a_0 \rightarrow K\bar{K})}{\text{Br}(a_0 \rightarrow \pi\eta)} = 0.23 \pm 0.05, \quad (6)$$

for $m_{a_0} = 0.999$ GeV, which gives $\text{Br}(a_0 \rightarrow K\bar{K}) = 0.187$. In another recent study [26], the WA102 collaboration reported the branching ratio

$$\Gamma(a_0 \rightarrow K\bar{K}) / \Gamma(a_0 \rightarrow \pi\eta) = 0.166 \pm 0.01 \pm 0.02, \quad (7)$$

which was determined from the measured branching ratio for the $f_1(1285)$ meson. In our present analysis, we use the results from [25], however, keeping in mind that this branching ratio $\text{Br}(a_0 \rightarrow K\bar{K})$ more likely gives an “upper limit” for the $a_0 \rightarrow K\bar{K}$ decay.

Thus, the other two parameters in the Flatté distribution C_F and $g_{a_0 K\bar{K}}$ can be found by solving the system of integral equations, for example, Eq. (3) for $\text{Br}(a_0 \rightarrow K\bar{K}) = 0.187$ and the unitarity condition (5). For our calculations, we choose either $\Gamma_{a_0 \pi\eta}(M_R) = 70$ or 50 MeV, which gives two sets of independent parameters $g_{a_0 K\bar{K}}$, $g_{a_0 \pi\eta}$, and C_F for a fixed branching ratio $\text{Br}(a_0 \rightarrow K\bar{K}) = 0.187$:

$$\text{set 1 } (\Gamma_{a_0 \pi\eta} = 70 \text{ MeV}) : \quad (8)$$

$$g_{a_0 K\bar{K}} = 2.3 \text{ GeV}, \quad g_{a_0 \pi\eta} = 2.2 \text{ GeV}, \quad C_F = 0.365;$$

$$\text{set 2 } (\Gamma_{a_0 \pi\eta} = 50 \text{ MeV}) : \quad (9)$$

$$g_{a_0 K\bar{K}} = 1.9 \text{ GeV}, \quad g_{a_0 \pi\eta} = 1.9 \text{ GeV}, \quad C_F = 0.354.$$

Note that, for the $K^+ K^-$ or $K^0 \bar{K}^0$ final state, one has to take into account an isospin factor for the coupling constant, i.e., $g_{a_0 K^+ K^-} = g_{a_0 K^0 \bar{K}^0} = g_{a_0 K\bar{K}} / \sqrt{2}$, whereas $g_{a_0 K^+ \bar{K}^0} = g_{a_0 K^- \bar{K}^0} = g_{a_0 K\bar{K}}$.

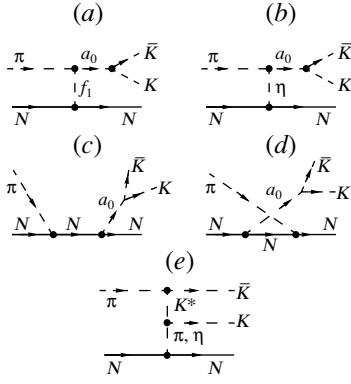


Fig. 1. (a–d) Diagrams for a_0 production in the reaction $\pi N \rightarrow a_0 N \rightarrow \bar{K} K$ near the threshold and (e) diagram for nonresonant $\bar{K} K$ “background” production.

3. THE REACTIONS $\pi N \rightarrow a_0 N$ AND $\pi N \rightarrow K \bar{K} N$

3.1. An Effective Lagrangian Approach

The simplest mechanisms for a_0 production in the reaction $\pi N \rightarrow a_0 N$ near the threshold are described by the pole diagrams shown in Figs. 1a–1d. It is known experimentally that a_0 couples strongly to the channels $\pi\eta$ and $\pi f_1(1285)$ because $\pi\eta$ is the dominant decay channel of a_0 , while πa_0 is one of the most important decay channels of $f_1(1285)$ [24]. The amplitudes, which correspond to the t -channel exchange of $\eta(550)$ and $f_1(1285)$ mesons (see Figs. 1b and 1a), can be written as

$$M_{\eta}^t(\pi^- p \rightarrow a_0^- p) = g_{\eta\pi a_0} g_{\eta NN} \bar{u}(p_2') \gamma_5 u(p_2) \quad (10)$$

$$\times \frac{1}{t - m_{\eta}^2} F_{\eta\pi a_0}(t) F_{\eta NN}(t),$$

$$M_{f_1}^t(\pi^- p \rightarrow a_0^- p) = g_{f_1\pi a_0} g_{f_1 NN} \quad (11)$$

$$\times (p_1 + p_1')_{\mu} \left(g_{\mu\nu} - \frac{q_{\mu} q_{\nu}}{m_{f_1}^2} \right) \bar{u}(p_2') \gamma_{\nu} \gamma_5 u(p_2)$$

$$\times \frac{1}{t - m_{f_1}^2} F_{f_1\pi a_0}(t) F_{f_1 NN}(t).$$

Here, p_1 and p_1' are the 4-momenta of π^- and a_0^- , whereas p_2 and p_2' are the 4-momenta of the initial and final protons, respectively; furthermore, $q = p_2' - p_2$ and $t = (p_2' - p_2)^2$. The functions F_j present form factors at the different vertices j ($j = f_1 NN, \eta NN$), which are taken of the monopole form

$$F_j(t) = \frac{\Lambda_j^2 - m_j^2}{\Lambda_j^2 - t}, \quad (12)$$

where Λ_j is a cutoff parameter. In the case of η exchange, we use $g_{\eta NN} = 6.1$ and $\Lambda_{\eta NN} = 1.5$ GeV

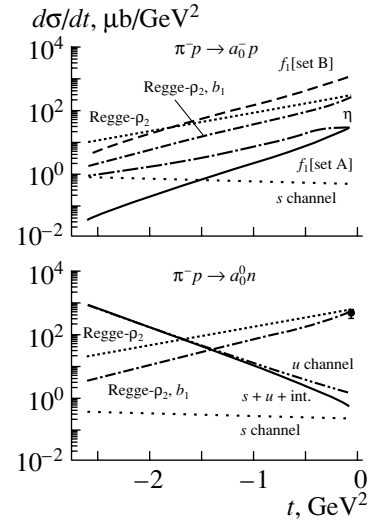


Fig. 2. The differential cross sections $d\sigma/dt$ for the reactions $\pi^- p \rightarrow a_0^- p$ and $\pi^- p \rightarrow a_0^0 n$ at 2.4 GeV/c. The long-dash-dotted line corresponds to the η exchange, and the solid and long-dashed lines (upper part) show the f_1 contributions within sets A and B, respectively. The rare-dotted and dash-double-dotted lines indicate the s and u channels, while the solid line (lower part) describes the coherent sum of s - and u -channel contributions including interference. The dotted and short-dash-dotted lines present the results within the ρ_2 and ρ_2, b_1 Regge exchange model, respectively (see text).

from [27] and $g_{a_0\pi\eta}$ is defined by (8). The contribution of the f_1 exchange is calculated for two parameter sets:

set A: $g_{f_1 NN} = 11.2$, $\Lambda_{f_1 NN} = 1.5$ GeV [28],
set B: $g_{f_1 NN} = 14.6$, $\Lambda_{f_1 NN} = 2.0$ GeV [29],
and $g_{f_1 a_0 \pi} = 2.5$ for both cases. The latter value for $g_{f_1 a_0 \pi}$ corresponds to $\Gamma(f_1 \rightarrow a_0 \pi) = 24$ MeV and $\text{Br}(f_1 \rightarrow a_0 \pi) = 34\%$.

In Fig. 2 (upper part), we show the differential cross sections $d\sigma/dt$ for the reaction $\pi^- p \rightarrow a_0^- p$ at 2.4 GeV/c corresponding to η (long-dash-dotted line) and f_1 exchanges with set A (solid line) and set B (long-dashed line). A soft cutoff parameter (set A) close to the mass of f_1 implies that all the contributions related to f_1 exchange become negligibly small. On the other hand, for the parameter values given by set B, the f_1 -exchange contribution is much larger than that from η exchange. Note that this large uncertainty in the cutoff presently cannot be controlled by data, and we will discuss the relevance of the f_1 -exchange contribution for all reactions separately throughout this study. For set B, the total cross section for the reaction $\pi^- p \rightarrow a_0^- p$ is about 0.5 mb at 2.4 GeV/c [cf. Fig. 3 (upper part)], while the forward differential cross section is about 1 mb/GeV².

The η and f_1 exchanges, however, do not contribute to the amplitude of the charge-exchange reaction $\pi^- p \rightarrow a_0^0 n$. In this case, we have to consider the contributions of the s - and u -channel diagrams (Figs. 1c and 1d):

$$M_N^s(\pi^- p \rightarrow a_0^0 n) = g_{a_0 NN} \frac{f_{\pi NN}}{m_\pi} \frac{1}{s - m_N^2} F_N(s) \quad (13)$$

$$\times p_{1\mu} \bar{u}(p_2') [(p_1 + p_2)_\alpha \gamma_\alpha + m_N] \gamma_\mu \gamma_5 u(p_2),$$

$$M_N^u(\pi^- p \rightarrow a_0^0 n) = g_{a_0 NN} \frac{f_{\pi NN}}{m_\pi} \frac{1}{u - m_N^2} F_N(u) \quad (14)$$

$$\times p_{1\mu} \bar{u}(p_2') \gamma_\mu \gamma_5 [(p_2 - p_1')_\alpha \gamma_\alpha + m_N] u(p_2),$$

where $s = (p_1 + p_2)^2$, $u = (p_2 - p_1')^2$, and m_N is the nucleon mass.

The πNN coupling constant is taken as $f_{\pi NN}^2/4\pi = 0.08$ [27], and the form factor for each virtual nucleon is taken in the so-called monopole form

$$F_N(u) = \frac{\Lambda_N^4}{\Lambda_N^4 + (u - m_N^2)^2}. \quad (15)$$

Following [18], we adopt here a cutoff parameter $\Lambda_N = 1.24$ GeV (see also discussion below).

The rare-dotted and dash-double-dotted lines in the lower part of Fig. 2 show the differential cross section for the charge-exchange reaction $\pi^- p \rightarrow a_0^0 n$ at 2.4 GeV/c corresponding to s - and u -channel diagrams, respectively. Due to isospin constraints, only the s channel contributes to the $\pi^- p \rightarrow a_0^- p$ reaction (rare-dotted line in the upper part of Fig. 2). In these calculations, the cutoff parameter $\Lambda_N = 1.24$ GeV and $g_{a_0 NN}^2/4\pi \simeq 1$ have been employed in line with the Bonn potential [27]. The solid line in the lower part of Fig. 2 describes the coherent sum of the s - and u -channel contributions, including the interference of the amplitudes. Except for the very forward region, the s -channel contribution (rare-dotted line) is rather small compared to the u channel for the charge-exchange reaction $\pi^- p \rightarrow a_0^0 n$, which may give a backward differential cross section of about 1 mb/GeV². The corresponding total cross section can be about 0.3 mb at this energy (cf. Fig. 3, middle part).

There is a single experimental point for the forward differential cross section of the reaction $\pi^- p \rightarrow a_0^0 n$ at 2.4 GeV/c ([30], lower part of Fig. 2),

$$\left. \frac{d\sigma}{dt}(\pi^- p \rightarrow a_0^0 n) \right|_{t \approx 0} = 0.49 \text{ mb/GeV}^2.$$

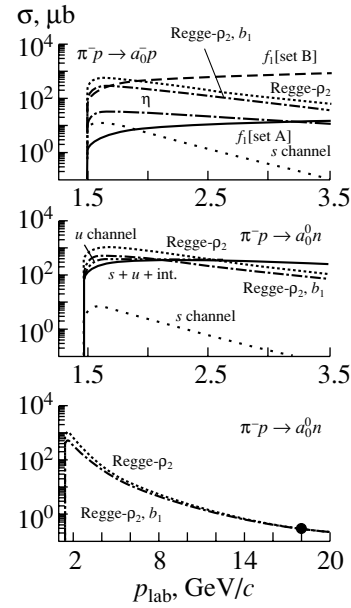


Fig. 3. The total cross sections for the reactions $\pi^- p \rightarrow a_0^- p$ and $\pi^- p \rightarrow a_0^0 n$ as a function of the incident momentum. The assignment of the curves is the same as in Fig. 2. The experimental data point at 18 GeV/c (lower part) is taken from [35].

Since in the forward region ($t \approx 0$) the s - and u -channel diagrams only give a smaller cross section, the charge-exchange reaction $\pi^- p \rightarrow a_0^0 n$ is most probably dominated at small t by the isovector $b_1(1^{+-})$ - and $\rho_2(2^{--})$ -meson exchanges (see, e.g., [11]). Though the couplings of these mesons to πa_0 and NN are not known, we can estimate $d\sigma(\pi^- p \rightarrow a_0^0 n)/dt$ in the forward region using the Regge pole model as developed by Achasov and Shestakov [12]. Note that the Regge pole model is expected to provide a reasonable estimate for the cross section at medium energies of about a few GeV and higher (see, e.g., [31, 32] and references therein).

3.2. The Regge Pole Model

The s -channel helicity amplitudes for the reaction $\pi^- p \rightarrow a_0^0 n$ can be written as

$$M_{\lambda_2' \lambda_2}(\pi^- p \rightarrow a_0^0 n) = \bar{u}_{\lambda_2'}(p_2') \quad (16)$$

$$\times \left[-A(s, t) + (p_1 + p_1')_\alpha \gamma_\alpha \frac{B(s, t)}{2} \right] \gamma_5 u_{\lambda_2}(p_2),$$

where the invariant amplitudes $A(s, t)$ and $B(s, t)$ do not contain kinematical singularities and (at fixed t and large s) are related to the helicity amplitudes as

$$M_{++} \approx -sB, \quad M_{+-} \approx \sqrt{t_{\min} - t}A. \quad (17)$$

The differential cross section then can be expressed through the helicity amplitudes in the standard way as

$$\begin{aligned} & \frac{d\sigma}{dt}(\pi^- p \rightarrow a_0^0 n) \\ &= \frac{1}{64\pi s} \frac{1}{(p_1^{\text{c.m.}})^2} (|M_{++}|^2 + |M_{+-}|^2). \end{aligned} \quad (18)$$

Usually, it is assumed that the reaction $\pi^- p \rightarrow a_0^0 n$ at high energies is dominated by the b_1 Regge pole exchange. However, as shown by Achasov and Shestakov [12], this assumption is not compatible with the angular dependence of $d\sigma(\pi^- p \rightarrow a_0^0 n)/dt$ observed at Serpukhov at 40 GeV/c [33, 34] and Brookhaven at 18 GeV/c [35]. The reason is that the b_1 Regge trajectory contributes only to the amplitude $A(s, t)$, giving a dip in differential cross section at forward angles, while the data show a clear forward peak in $d\sigma(\pi^- p \rightarrow a_0^0 n)/dt$ at both energies. To interpret this phenomenon, Achasov and Shestakov [12] introduced a ρ_2 Regge pole exchange conspiring with its daughter trajectory. Since the ρ_2 Regge trajectory contributes to both invariant amplitudes, $A(s, t)$ and $B(s, t)$, its contribution does not vanish at the forward scattering angle $\theta = 0$, thus giving a forward peak due to the term $|M_{++}|^2$ in $d\sigma/dt$. At the same time, the contribution of the ρ_2 daughter trajectory to the amplitude $A(s, t)$ is necessary to cancel the kinematical pole at $t = 0$ introduced by the ρ_2 main trajectory (conspiracy effect). In this model, the s -channel helicity amplitudes can be expressed through the b_1 and the conspiring ρ_2 Regge trajectories exchange as

$$\begin{aligned} M_{++} &\approx M_{++}^{\rho_2}(s, t) \\ &= \gamma_{\rho_2}(t) \exp\left[-i\frac{\pi}{2}\alpha_{\rho_2}(t)\right] \left(\frac{s}{s_0}\right)^{\alpha_{\rho_2}(t)}, \end{aligned} \quad (19)$$

$$\begin{aligned} M_{+-} &\approx M_{+-}^{b_1}(s, t) = \sqrt{(t_{\min} - t)/s_0} \gamma_{b_1}(t) \\ &\times i \exp\left[-i\frac{\pi}{2}\alpha_{b_1}(t)\right] \left(\frac{s}{s_0}\right)^{\alpha_{b_1}(t)}, \end{aligned} \quad (20)$$

where $\gamma_{\rho_2}(t) = \gamma_{\rho_2}(0) \exp(b_{\rho_2} t)$, $\gamma_{b_1}(t) = \gamma_{b_1}(0) \times \exp(b_{b_1} t)$, $t_{\min} \approx -m_N^2(m_{a_0}^2 - m_\pi^2)/s^2$, and $s_0 \approx 1 \text{ GeV}^2$, while the meson Regge trajectories have the linear form $\alpha_j(t) = \alpha_j(0) + \alpha_j'(0)t$.

Achasov and Shestakov describe the Brookhaven data on the t distribution at 18 GeV/c for $-t_{\min} \leq -t \leq 0.6 \text{ GeV}^2$ [35] by the expression

$$\frac{dN}{dt} = C_1 \left[e^{\Lambda_1 t} + (t_{\min} - t) \frac{C_2}{C_1} e^{\Lambda_2 t} \right], \quad (21)$$

where the first and second terms describe the ρ_2 and b_1 exchanges, respectively. They found two fits: (i)

$\Lambda_1 = 4.7 \text{ GeV}^{-2}$, $C_2/C_1 = 0$; (ii) $\Lambda_1 = 7.6 \text{ GeV}^{-2}$, $C_2/C_1 \approx 2.6 \text{ GeV}^{-2}$, $\Lambda_2 = 5.8 \text{ GeV}^{-2}$. This implies that at 18 GeV/c the b_1 contribution yields only 1/3 of the integrated cross section. Moreover, using the available data on the reaction $\pi^- p \rightarrow a_2^0(1320)n$ at 18 GeV/c and comparing them with the data on the $\pi^- p \rightarrow a_0^0 n$ reaction, they estimated the total and forward differential cross sections $\sigma(\pi^- p \rightarrow a_0^0 n \rightarrow \pi^0 \eta n) \approx 200 \text{ nb}$ and $[d\sigma(\pi^- p \rightarrow a_0^0 n \rightarrow \pi^0 \eta n)/dt]_{t=0} \approx 940 \text{ nb/GeV}^2$. Taking $\text{Br}(a_0^0 \rightarrow \pi^0 \eta) \approx 0.8$, we find $\sigma(\pi^- p \rightarrow a_0^0 n) \approx 0.25 \mu\text{b}$ and $[d\sigma(\pi^- p \rightarrow a_0^0 n)/dt]_{t=0} \approx 1.2 \mu\text{b/GeV}^2$.

In this way, all the parameters of the Regge model can be fixed, and we will employ it for the energy dependence of the $\pi^- p \rightarrow a_0^0 n$ cross section to obtain an estimate at lower energies too.

The mass of $\rho_2(2^{--})$ is expected to be about 1.7 GeV (see [36] and references therein), and the slope of the meson Regge trajectory in the case of light (u, d) quarks is 0.9 GeV^{-2} [37]. Therefore, the intercept of the ρ_2 Regge trajectory is $\alpha_{\rho_2}(0) = 2 - 0.9m_{\rho_2}^2 \approx -0.6$. Similarly—in the case of the b_1 trajectory—we have $\alpha_{b_1}(0) \approx -0.37$. At forward angles, we can neglect the contribution of the b_1 exchange (see discussion above) and write the energy dependence of the differential cross section in the form

$$\begin{aligned} & \frac{d\sigma_{\text{Regge}}}{dt}(\pi^- p \rightarrow a_0^0 n) \Big|_{t=0} \approx \frac{d\sigma_{\rho_2}}{dt} \Big|_{t=0} \\ & \sim \frac{1}{(p_1^{\text{c.m.}})^2} \left(\frac{s}{s_0}\right)^{-2.2}. \end{aligned} \quad (22)$$

This provides the following estimate for the forward differential cross section at 2.4 GeV/c,

$$\frac{d\sigma_{\text{Regge}}}{dt}(\pi^- p \rightarrow a_0^0 n) \Big|_{t=0} \approx 0.6 \text{ mb/GeV}^2, \quad (23)$$

which is in agreement with the experimental data point [30] (lower part of Fig. 2). Since the b_1 and ρ_2 Regge trajectories have isospin 1, their contribution to the cross section for the reaction $\pi^- p \rightarrow a_0^- p$ is a factor of 2 smaller,

$$\frac{d\sigma_{\text{Regge}}}{dt}(\pi^- p \rightarrow a_0^- p) = \frac{1}{2} \frac{d\sigma_{\text{Regge}}}{dt}(\pi^- p \rightarrow a_0^0 n). \quad (24)$$

In Fig. 2, the dotted lines show the resulting differential cross sections for $d\sigma_{\text{Regge}}(\pi^- p \rightarrow a_0^- p)/dt$ (upper part) and $d\sigma_{\text{Regge}}(\pi^- p \rightarrow a_0^0 n)/dt$ (lower part) at 2.4 GeV/c corresponding to ρ_2 Regge exchange, whereas the short-dash-dotted lines indicate the contribution for ρ_2 and b_1 Regge trajectories. For $t \rightarrow 0$, both Regge parametrizations agree; however,

at large $|t|$ the solution including the b_1 exchange gives a smaller cross section. The cross section $d\sigma_{\text{Regge}}(\pi^-p \rightarrow a_0^-p)/dt$ in the forward region exceeds the contributions of η , f_1 (set A), and s -channel exchanges, but is a few times smaller than the f_1 -exchange contribution for set B. On the other hand, the cross section $d\sigma_{\text{Regge}}(\pi^-p \rightarrow a_0^0n)/dt$ is much larger than the s - and u -channel contributions in the forward region, but much smaller than the u -channel contribution in the backward region.

The integrated cross sections for $\pi^-p \rightarrow a_0^-p$ (upper part) and $\pi^-p \rightarrow a_0^0n$ (middle and lower part) for the Regge model are shown in Fig. 3 as a function of the pion laboratory momentum by dotted curves for ρ_2 exchange and by short-dash-dotted curves for ρ_2 , b_1 trajectories. In the few-GeV region, the cross sections are comparable with the u -channel contribution. At higher energies, the Regge cross section decreases as $s^{-3.2}$ in contrast to the non-Reggeized f_1 -exchange contribution, which increases with energy and seems to be too large at 2.5 GeV/ c for parameters from the set B. We thus expect parameter set B to be unrealistic.

The main conclusions of this subsection are as follows. In the region of a few GeV, the dominant mechanisms of a_0 production in the reaction $\pi N \rightarrow a_0N$ is the u -channel nucleon exchange (cf. middle part of Fig. 3). A similar cross section ($\simeq 0.4$ – 1.0 mb) is predicted by the Regge model with conspiring ρ_2 (or ρ_2 and b_1) exchanges, normalized to the Brookhaven data at 18 GeV/ c (lower part of Fig. 3). The contributions of s -channel nucleon and t -channel η -meson exchanges are small (cf. upper and middle parts of Fig. 3).

3.3. Possible Signals of a_0 Production in the Reaction $\pi N \rightarrow K\bar{K}N$

In Fig. 4, we show the existing experimental data on the reactions $\pi^-p \rightarrow nK^+K^-$, $\pi^-p \rightarrow nK^0\bar{K}^0$, $\pi^+p \rightarrow pK^+\bar{K}^0$, and $\pi^-p \rightarrow pK^0K^-$ taken from [38]. The solid curves describe s - and u -channel contributions, calculated using the dipole nucleon form factor ($F_N^2(u)$) with $\Lambda_N = 1.35$ GeV. The short-dashed and long-dashed curves describe η and f_1 t -channel exchanges, respectively. Two different choices of the Regge pole model are shown by the dash-dotted curves, which describe ρ_2 exchange (upper) and ρ_2 , b_1 exchange (lower). The crossed solid curves display the background contribution (see Fig. 1e), which was calculated using parameters of the K^* exchange from the Jülich model [3]. It is important that, for the reactions $\pi^+p \rightarrow pK^+\bar{K}^0$ and $\pi^-p \rightarrow pK^0K^-$, where the $K\bar{K}$ pair has isospin 1, the main contributions come from P -wave $K\bar{K}$ -pair production from

the $\pi\pi$ state and from S -wave $K\bar{K}$ -pair production from the $\eta\pi$ state. These selection rules follow from G -parity conservation (note that the G parity of the $K\bar{K}$ system with orbital momentum L and isospin I is given by $(-1)^{L+I}$). At the same time, for the reactions $\pi^-p \rightarrow nK^+K^-$ and $\pi^-p \rightarrow nK^0\bar{K}^0$, the essential contribution to the background stems from S -wave $K\bar{K}$ -pair production from the isoscalar $\pi\pi$ state. Let us note that the parametrization of the total cross sections for the reactions $\pi N \rightarrow K\bar{K}N$ has been discussed previously in [39]. Here, we also analyze contributions from different channels to the total cross sections.

The most important point is that for all the reactions the background is essentially below the data at the c.m. energy release $Q \leq 300$ MeV. In the case of the reactions $\pi^+p \rightarrow pK^+\bar{K}^0$ and $\pi^-p \rightarrow pK^0K^-$ this, in our opinion, can only be due to a contribution of a_0 . Of course, in the reactions $\pi^-p \rightarrow nK^+K^-$ and $\pi^-p \rightarrow nK^0\bar{K}^0$, both scalar mesons, f_0 and a_0 , can contribute. In a series of bubble chamber experiments performed in the 1960–1970s, a structure was reported in the mass distribution of the $K_S^0K_S^0$ system produced in the reaction $\pi^-p \rightarrow nK_S^0K_S^0$ (see, e.g., [40] and references therein). Usually, this structure was attributed to $f_0(980)$. In our previous work, we used the data on $\pi^-p \rightarrow nf_0 \rightarrow nK_S^0K_S^0$ to find a restriction on the branching $\text{Br}(f_0 \rightarrow K\bar{K})$ [41]. We see here from Fig. 4 (upper right) that an important contribution to the cross section of the reaction $\pi^-p \rightarrow nK^0\bar{K}^0$ at $Q \leq 300$ MeV also comes from a_0 . We cannot exclude that there can also be some contribution from $a_0(980)$ at $Q \geq 300$ MeV. If this is really the case, our restriction on $\text{Br}(f_0 \rightarrow K\bar{K})$ [41] has to be corrected. This problem, however, requires further analysis.

Let us note that the amplitude corresponding to the Feynman diagram in Fig. 1e would predict a sharply rising cross section for $Q \geq 400$ MeV. To suppress this unrealistic behavior, we used a Reggeized K^* propagator multiplying the Feynman propagator of the vector meson in all the amplitudes by the Regge power $(s/s_0)^{(\alpha_{K^*}(0)-1)}$ with $\alpha_{K^*}(0) \simeq 0.25$ and $\sqrt{s_0} = 2m_K + m_N$. The background curves are in reasonable agreement with the data on the reactions $\pi^+p \rightarrow pK^+\bar{K}^0$ and $\pi^-p \rightarrow pK^0K^-$ at $Q \geq 400$ MeV (see the crossed solid curves in the two lower panels of Fig. 4).

The Regge pole model for a_0 production, especially the set with b_1 and ρ_2 exchange, is in good agreement with the data for all the reactions at $Q \leq 300$ MeV, giving a cross section of the reaction $\pi N \rightarrow a_0N \rightarrow K\bar{K}N$ of about 20–30 μb at $Q \simeq 100$ –300 MeV. At

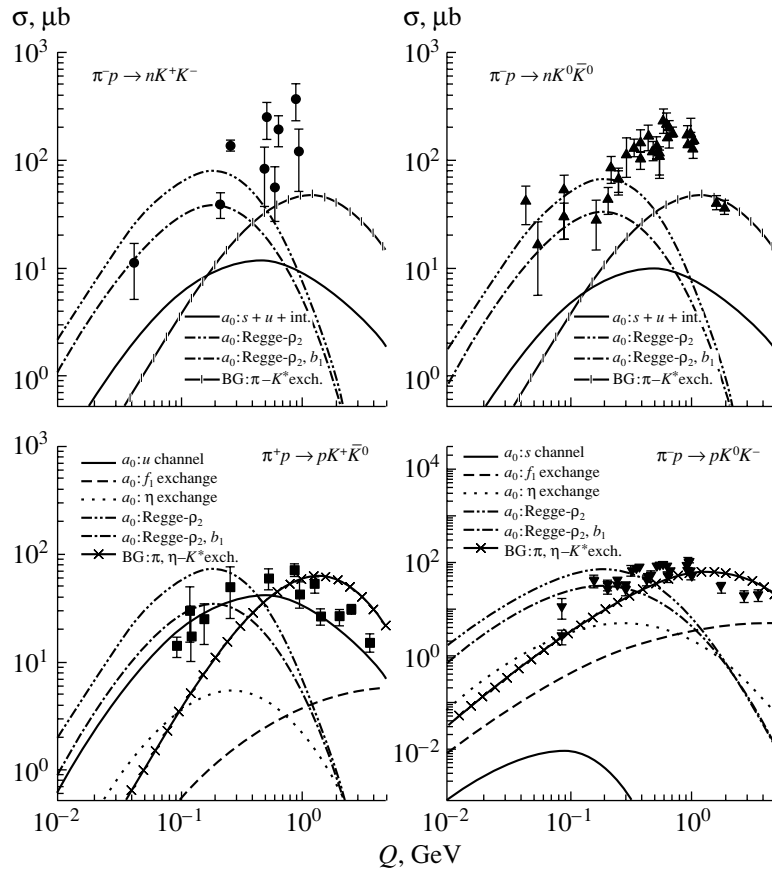


Fig. 4. The total cross sections for the reactions $\pi^-p \rightarrow nK^+K^-$, $\pi^-p \rightarrow nK^0\bar{K}^0$, $\pi^+p \rightarrow pK^+\bar{K}^0$, and $\pi^-p \rightarrow pK^0K^-$ as a function of $Q = \sqrt{s} - \sqrt{s_0}$. Experimental data are taken from [38]. The solid curves describe s - and u -channel contributions, calculated with the dipole nucleon form factor $F_N^2(u)$ with $\Lambda_N = 1.35$ GeV. The short-dashed and long-dashed curves describe η and f_1 t -channel exchanges, respectively. Two different choices of the Regge pole model are shown by the dash-dotted curves which describe ρ_2 exchange (upper) and conspiring ρ_2, b_1 exchange (lower). The crossed solid curves show the background contribution from diagram in Fig. 1e.

larger Q , it drops very fast. The u -channel contribution is also in good agreement with the data on the reaction $\pi^+p \rightarrow pK^+\bar{K}^0$, but the coherent sum of the u - and s -channel contributions is below the data for the reactions $\pi^-p \rightarrow nK^+K^-$ and $\pi^-p \rightarrow nK^0\bar{K}^0$. The t -channel η - and f_1 -exchange contributions are small and can be neglected.

Note that both invariant mass distributions of the $K^-\bar{K}^0$ and $K_S^0K_S^0$ systems presented in [40] show a resonance-like structure near the $K\bar{K}$ threshold at $Q \leq 300$ MeV. However, because of a comparatively small number of events for each fixed initial momentum, those distributions are averaged over a large interval of about 1 GeV/ c in p_{lab} . Unfortunately, those distributions cannot be directly compared with theoretical ones at any fixed Q , especially in the near-threshold region. In order to give another strong argument that the a_0 contribution is really necessary to explain the existing experimental data, let us consider the energy dependence of the total cross section of

the reaction $\pi^-p \rightarrow pK^-\bar{K}^0$. Averaging the existing data from [38] versus p_{lab} over the intervals 2.0 ± 0.15 and 3.0 ± 0.15 GeV/ c , we find $\sigma_{\text{av}} = 34.9 \pm 3.3$ and 73.8 ± 7.6 μb , respectively. The ratio of those cross sections is equal to $R_{21} \simeq 2.1 \pm 0.05$. The energy behavior of the background contribution in our model is $\sigma_{\text{bg}} \sim Q^{2.3}$. If we assume that, in the interval of $Q = 250\text{--}630$ MeV (which corresponds to the interval of $p_{\text{lab}} = 2\text{--}3$ GeV/ c), the background contribution is present only, we get $R_{21}^{\text{bg}} \simeq 5.5$. This means that at 3 GeV/ c we should expect a cross section of $\simeq 200$ μb instead of ~ 70 μb . Evidently, experimental data are inconsistent with this assumption.

Let us formulate the main conclusions of this subsection. The existing data on the reactions $\pi^+p \rightarrow pK^+\bar{K}^0$ and $\pi^-p \rightarrow pK^0K^-$ give rather strong evidence that, at low energy above threshold ($Q \leq 300$ MeV), they are dominated by a_0 production. The same is also true for the reactions $\pi^-p \rightarrow nK^+K^-$

Coefficients in Eq. (25) for different mechanisms of the $pp \rightarrow ppa_0^0$, $pp \rightarrow pna_0^+$, $pn \rightarrow ppa_0^-$, and $pn \rightarrow pna_0^0$ reactions

| Reaction j | Mechanism α | $\xi_{j(\alpha)}^\pi[ab; cd]$ | $\xi_{j(\alpha)}^\pi[ab; dc]$ | $\xi_{j(\alpha)}^\pi[ba; dc]$ | $\xi_{j(\alpha)}^\pi[ba; cd]$ |
|--------------------------|--------------------|-------------------------------|-------------------------------|-------------------------------|-------------------------------|
| $pp \rightarrow ppa_0^0$ | $t(\eta), t(f_1)$ | $+1/\sqrt{2}$ | $-1/\sqrt{2}$ | $+1/\sqrt{2}$ | $-1/\sqrt{2}$ |
| | $s(N)$ | $+1/\sqrt{2}$ | $-1/\sqrt{2}$ | $+1/\sqrt{2}$ | $-1/\sqrt{2}$ |
| | $u(N)$ | $+1/\sqrt{2}$ | $-1/\sqrt{2}$ | $+1/\sqrt{2}$ | $-1/\sqrt{2}$ |
| | Regge | 0 | 0 | 0 | 0 |
| $pp \rightarrow pna_0^+$ | $t(\eta), t(f_1)$ | $-\sqrt{2}$ | 0 | 0 | $+\sqrt{2}$ |
| | $s(N)$ | 0 | $+\sqrt{2}$ | $-\sqrt{2}$ | 0 |
| | $u(N)$ | $+2\sqrt{2}$ | $-\sqrt{2}$ | $+\sqrt{2}$ | $-2\sqrt{2}$ |
| | Regge | -1 | +1 | -1 | +1 |
| $pn \rightarrow ppa_0^-$ | $t(\eta), t(f_1)$ | +1 | -1 | 0 | 0 |
| | $s(N)$ | -2 | +2 | -1 | +1 |
| | $u(N)$ | 0 | 0 | +1 | -1 |
| | Regge | $+1/\sqrt{2}$ | $-1/\sqrt{2}$ | $-1/\sqrt{2}$ | $+1/\sqrt{2}$ |
| $pn \rightarrow pna_0^0$ | $t(\eta), t(f_1)$ | -1 | 0 | +1 | 0 |
| | $s(N)$ | -1 | -2 | +1 | +2 |
| | $u(N)$ | -1 | +2 | +1 | -2 |
| | Regge | 0 | $+\sqrt{2}$ | 0 | $-\sqrt{2}$ |

and $\pi^-p \rightarrow nK^0\bar{K}^0$, where some smaller contribution of f_0 may also be present. The value of the a_0 -production cross section is reasonably described by the Regge pole model with ρ_2 , b_1 exchange as proposed by Achasov and Shestakov [12]. The u -channel exchange mechanism also gives a reasonable value of the cross section.

4. THE REACTION $NN \rightarrow NN a_0$

4.1. An Effective Lagrangian Approach with One-Pion Exchange

We consider a_0^0 , a_0^+ , a_0^- production in the reactions $j = pp \rightarrow ppa_0^0$, $pp \rightarrow pna_0^+$, $pn \rightarrow ppa_0^-$, and $pn \rightarrow pna_0^0$ using the effective Lagrangian approach with one-pion exchange (OPE). For the elementary $\pi N \rightarrow Na_0$ transition amplitude, we take into account different mechanisms α corresponding to t -channel diagrams with $\eta(550)$ - and $f_1(1285)$ -meson exchanges ($\alpha = t(\eta), t(f_1)$) as well as s - and u -channel graphs with an intermediate nucleon ($\alpha = s(N), u(N)$) (cf. [18]). The corresponding diagrams are shown in Fig. 5. The invariant amplitude of the $NN \rightarrow NN a_0$ reaction then is the sum of the four basic terms (diagrams in Fig. 5) with permutations of nucleons in the initial and final states

$$\mathcal{M}_{j(\alpha)}^\pi[ab; cd] = \xi_{j(\alpha)}^\pi[ab; cd] \mathcal{M}_\alpha^\pi[ab; cd] \quad (25)$$

$$+ \xi_{j(\alpha)}^\pi[ab; dc] \mathcal{M}_\alpha^\pi[ab; dc] + \xi_{j(\alpha)}^\pi[ba; dc] \mathcal{M}_\alpha^\pi[ba; dc] + \xi_{j(\alpha)}^\pi[ba; cd] \mathcal{M}_\alpha^\pi[ba; cd],$$

where the coefficients $\xi_{j(\alpha)}^\pi$ are given in the table. The amplitudes for the t -channel exchange with $\eta(550)$ and $f_1(1285)$ mesons are given by

$$\begin{aligned} \mathcal{M}_{t(\eta)}^\pi[ab; cd] &= g_{a_0\eta\pi} F_{a_0\eta\pi} \quad (26) \\ &\times ((p_a - p_c)^2, (p_d - p_b)^2) g_{\eta NN} F_\eta ((p_a - p_c)^2) \\ &\times \frac{1}{(p_a - p_c)^2 - m_\eta^2} \bar{u}(p_c) \gamma_5 u(p_a) \Pi(p_b; p_d), \end{aligned}$$

$$\begin{aligned} \mathcal{M}_{t(f_1)}^\pi[ab; cd] &= -g_{a_0 f_1 \pi} F_{a_0 f_1 \pi} \quad (27) \\ &\times ((p_a - p_c)^2, (p_d - p_b)^2) g_{f_1 NN} F_{f_1} ((p_a - p_c)^2) \\ &\times \frac{1}{(p_a - p_c)^2 - m_{f_1}^2} (p_a - p_c + 2(p_b - p_d))_\mu \\ &\times \left(g_{\mu\nu} - \frac{(p_a - p_c)_\mu (p_a - p_c)_\nu}{m_{f_1}^2} \right) \\ &\times \bar{u}(p_c) \gamma_5 \gamma_\nu u(p_a) \Pi(p_b; p_d), \end{aligned}$$

with

$$\Pi(p_b; p_d) = \frac{f_{\pi NN}}{m_\pi} F_\pi ((p_b - p_d)^2) (p_b - p_d)_\beta \quad (28)$$

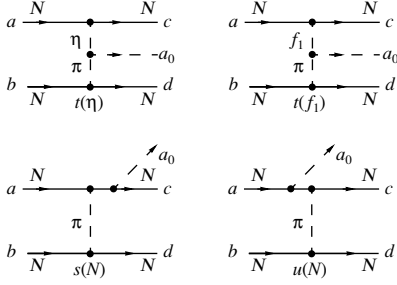


Fig. 5. Diagrams for a_0 production in the reaction $NN \rightarrow a_0NN$.

$$\times \bar{u}(p_d)\gamma_5\gamma_\beta u(p_b) \frac{1}{(p_b - p_d)^2 - m_\pi^2}.$$

The amplitudes for the s and u channels (lower part of Fig. 5) are given as

$$\begin{aligned} \mathcal{M}_{s(N)}^\pi[ab; cd] &= \Pi(p_b; p_d) \quad (29) \\ &\times \frac{f_{\pi NN}}{m_\pi} F_\pi((p_d - p_b)^2) g_{a_0 NN} \\ &\times \frac{F_N((p_a + p_b - p_d)^2)}{(p_a + p_b - p_d)^2 - m_N^2} (p_d - p_b)_\mu \bar{u}(p_c) \\ &\times [(p_a + p_b - p_d)\delta\gamma_\delta + m_N]\gamma_5\gamma_\mu u(p_a), \\ \mathcal{M}_{u(N)}^\pi[ab; cd] &= \Pi(p_b; p_d) \quad (30) \\ &\times \frac{f_{\pi NN}}{m_\pi} F_\pi((p_d - p_b)^2) g_{a_0 NN} \\ &\times \frac{F_N((p_c + p_d - p_b)^2)}{(p_c + p_d - p_b)^2 - m_N^2} (p_d - p_b)_\mu \bar{u}(p_c)\gamma_5\gamma_\mu \\ &\times [(p_c + p_d - p_b)\delta\gamma_\delta + m_N]u(p_a). \end{aligned}$$

Here, p_a, p_b and p_c, p_d are the 4-momenta of the initial and final nucleons, respectively. As in the previous section, we mostly employ coupling constants and form factors from the Bonn–Jülich potentials (see, e.g., [27, 28, 42]).

For the form factors at the $a_0 f_1 \pi$ (as well as $a_0 \eta \pi$) vertex, factorized forms are applied following the assumption from [43, 44],

$$F_{a_0 f_1 \pi}(t_1, t_2) = F_{f_1 NN}(t_1) F_{\pi NN}(t_2), \quad (31)$$

where $F_{f_1 NN}(t), F_{\pi NN}(t)$ are taken in the monopole form (see previous section). Usually, the cutoff parameter $\Lambda_{\pi NN}$ is taken in the interval 1–1.3 GeV. Here, we take $\Lambda_{\pi NN} = 1.05$ GeV (see also the discussion in [19]).

As shown in the analysis of [18], the contribution of the η exchange to the amplitude $\pi N \rightarrow a_0 N$ is small (cf. also Section 3). Note that in [45] only this mechanism was taken into account for the reaction $pn \rightarrow pp a_0^-$. Here, we also include the η exchange

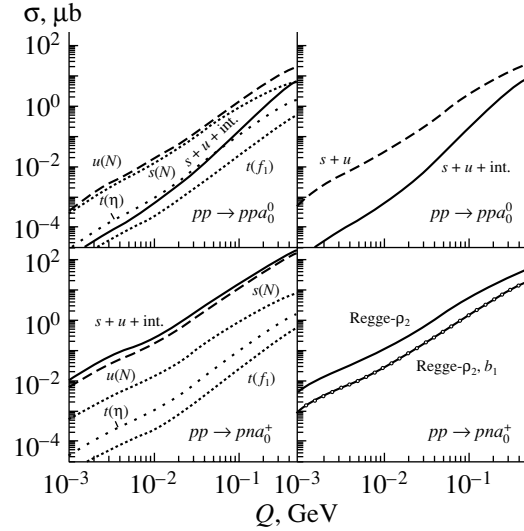


Fig. 6. The total cross sections for the reactions $pp \rightarrow ppa_0^0$ and $pp \rightarrow pna_0^+$ as a function of the excess energy $Q = \sqrt{s} - \sqrt{s_0}$ calculated with FSI.

because it might be noticeable in those isospin channels where a strong destructive interference of u - and s -channel terms can occur (see below).

Since we have two nucleons in the final state, it is necessary to take into account their final-state interaction (FSI), which has some influence on meson production near the threshold. For this purpose, we adopt the FSI model from [46] based on the (realistic) Paris potential. We use, however, the enhancement factor $F_{NN}(q_{NN})$ —as given by this model—only in the region of small relative momenta of the final nucleons $q_{NN} \leq q_0$, where it is larger than 1. Having in mind that this factor is rather uncertain at larger q_{NN} , where, for example, contributions of nonnucleon intermediate states to the loop integral might be important, we assume that $F_{NN}(q_{NN}) = 1$ for $q_{NN} \geq q_0$.

In Fig. 6, we show the total cross section as a function of the energy excess $Q = \sqrt{s} - \sqrt{s_0}$ for the reactions $pp \rightarrow ppa_0^0$ (upper part) and $pp \rightarrow pna_0^+$ (lower part). As seen from Fig. 6, the u and s channels give the dominant contribution; the $t(f_1)$ channel is small for both isospin reactions. For the reaction $pp \rightarrow pna_0^+$, the Regge exchange contribution (extended to low energies) becomes important. For the $pp \rightarrow ppa_0^0$ channel, the Regge model predicts no contribution from ρ_2 and ρ_2, b_1 exchanges due to isospin arguments (i.e., the vertex with a coupling of three neutral components of isovectors vanishes); thus, only $s, u, t(\eta)$, and $t(f_1)$ channels are plotted in the upper part of Fig. 6.

Here, we have to point out the influence of the interference between the s and u channels. According to the isospin coefficients from the OPE model presented in the table, the phase (of interference α) between the s and u channels $\mathcal{M}_{s(N)}^\pi + \exp(-i\alpha)\mathcal{M}_{u(N)}^\pi$ is equal to zero; i.e., the sign between $\mathcal{M}_{s(N)}^\pi$ and $\mathcal{M}_{u(N)}^\pi$ is “plus.” The solid curves in Fig. 6 indicate the coherent sum of $s(N)$ and $u(N)$ channels including the interference of the amplitudes ($s + u + \text{int.}$). One can see that, for the $pp \rightarrow pna_0^+$ reaction, the interference is positive and increases the cross section, whereas, for the $pp \rightarrow ppa_0^0$ channel, the interference is strongly destructive since we have identical particles in the initial and final states and the contributions of s and u channels are very similar.

Here, we would like to comment on an extension of the OPE model to a one-boson exchange (OBE) approximation, i.e., accounting for the exchange of σ , ρ , ω , \dots mesons as well as for multimeson exchanges. Generally speaking, the total cross section of a_0 production should contain the sum of all the contributions:

$$\sigma(NN \rightarrow NN a_0) = \sum_j \sigma_j,$$

where $j = \pi, \sigma, \rho, \omega, \dots$. Depending on their cutoff parameters, the heavier meson exchanges might give a comparable contribution to the total cross section for a_0 production. An important point, however, is that, near threshold (e.g., $Q \leq 0.3\text{--}0.6$ GeV), the energy behavior of all those contributions is the same, i.e., it is proportional to the three-body phase space $\sigma_j \sim Q^2$ (when the FSI is switched off and the narrow resonance width limit is taken). In this respect, we can consider the OPE as an effective one and normalize it to the experimental cross section by choosing an appropriate value of Λ_π . The most appropriate choice for Λ_π is about 1–1.3 GeV. Another question is related to the isospin of the effective exchange. As is known from a series of papers on the reactions $NN \rightarrow NN X$, $X = \eta, \eta', \omega, \phi$, the most important contributions to the corresponding cross sections near the threshold come from π and ρ exchanges (see, e.g., the review [47] and references therein). In line with those results, we assume here that the dominant contribution to the cross section of the reaction $NN \rightarrow NN a_0$ also comes from the isovector exchanges (like π and ρ). In principle, it is also possible that some baryon resonances may contribute. However, there is no information about resonances that couple to the $a_0 N$ system. Our assumptions thus enable us to make exploratory estimates of the a_0 -production cross section without introducing free parameters that would be out of control by existing data. The model can be extended

accordingly when new data on a_0 production become available.

Another important question is related to the choice of the form factor for a virtual nucleon, which—in line with the Bonn–Jülich potentials—we choose as given by (15), which corresponds to monopole form factors at the vertices. In the literature, furthermore, dipole-like form factors (at the vertices) are also often used (cf. [44, 47, 48]). However, there are no strict rules for the “correct” power of the nucleon form factor. In physics terms, the actual choice of the power should be irrelevant; we may have the same predictions for any reasonable choice of the power if the cutoff parameter Λ_N is fixed accordingly. Note that Λ_N may also depend on the type of mesons involved at the vertices. In our previous work [18], we have fixed Λ_N for the monopole related form factor (15) in the interval 1.2–1.3 GeV fitting the forward differential cross section of the reaction $pp \rightarrow da_0^+$ from [49]. On the other hand, the same data can be described rather well using a dipole form factor (at the vertices) with $\Lambda_N = 1.55\text{--}1.6$ GeV. If we employ this dipole form factor with $\Lambda_N = 1.55\text{--}1.6$ GeV in the present case, we obtain practically identical predictions for the cross sections of the channels $pp \rightarrow pna_0^+$, $pn \rightarrow pna_0^0$, and $pn \rightarrow ppa_0^-$, where the u -channel mechanism is dominant and u – s interference is not too important. In the case of the channel $pp \rightarrow ppa_0^0$, we obtain cross sections up to a factor of 2 larger for the dipole-like form factor in comparison to the monopole one. This is related to the strong destructive interference of the s - and u -exchange mechanisms, which slightly depends on the type of form factor used. However, our central result, that the cross section for the pna_0^+ final channel is about an order of magnitude higher than the ppa_0^0 channel in pp collisions, is robust (within less than a factor of 2) with respect to different choices of the form factor.

As seen from Fig. 6, we get the largest cross section for the $pp \rightarrow pna_0^+$ isospin channel. For this reaction, the u channel gives the dominant contribution; the s -channel cross section is small such that the interference is not so essential as for the $pp \rightarrow ppa_0^0$ reaction.

As was already discussed in our previous study [18], an effective Lagrangian model (ELM) cannot be extrapolated to high energies because it predicts the elementary amplitude $\pi N \rightarrow a_0 N$ to rise fast. Therefore, such a model can only be employed not far from the threshold. On the other hand, the Regge model is valid at large energies and we have to worry about how close to the threshold we can extrapolate corresponding amplitudes. According to duality arguments, one can expect that the Regge amplitude can be applied at low energy, too, if the reaction

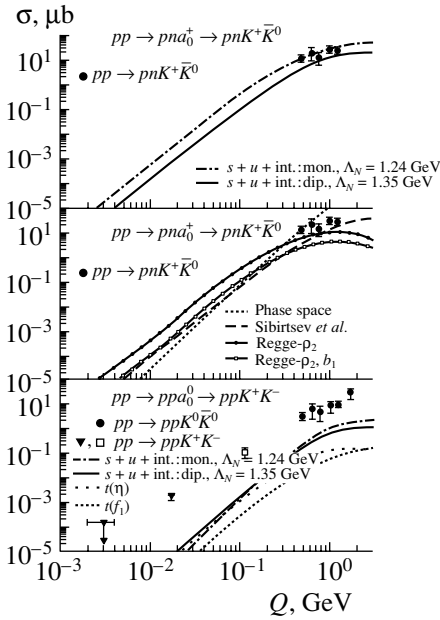


Fig. 7. The calculated total cross sections for the reactions $pp \rightarrow ppa_0^+ \rightarrow ppK^+\bar{K}_0^-$ and $pp \rightarrow pna_0^+ \rightarrow ppK^+\bar{K}_0^-$ in comparison to the experimental data as functions of $Q = \sqrt{s} - \sqrt{s_0}$. For more details, see the text.

$\pi N \rightarrow a_0 N$ does not contain essential s -channel resonance contributions. In this case, the Regge model might give a realistic estimate of the $\pi N \rightarrow a_0 N$ and $NN \rightarrow NN a_0$ amplitudes even near the threshold.

Anyway, as we have shown in [18] (see also Section 3), the Regge and u -channel model give quite similar results for the $\pi^- p \rightarrow a_0^0 n$ cross section in the threshold region; some differences in the cross sections of the reactions $NN \rightarrow NN a_0$ —as predicted by those two models—can be attributed to differences in the isospin factors and effects of NN antisymmetrization, which is important near the threshold (the latter was ignored in the Regge model formulated for larger energies).

4.2. Reaction $NN \rightarrow NN a_0 \rightarrow NNK\bar{K}$

4.2.1. Numerical results for the total cross section. In the upper part of Fig. 7, we display the calculated total cross section [within parameter set 1 (8)] for the reaction $pp \rightarrow pna_0^+ \rightarrow pnK^+\bar{K}_0^-$ in comparison to the experimental data for $pp \rightarrow pnK^+\bar{K}_0^-$ (dots) from [38] as a function of the excess energy $Q = \sqrt{s} - \sqrt{s_0}$. The dash-dotted and solid curves in Fig. 7 correspond to the coherent sum of $s(N)$ and $u(N)$ channels with interference ($s + u + \text{int.}$), calculated with a monopole form of the form factor (15) with $\Lambda_N = 1.24$ GeV and with a dipole form ($F_N(u)^2$)

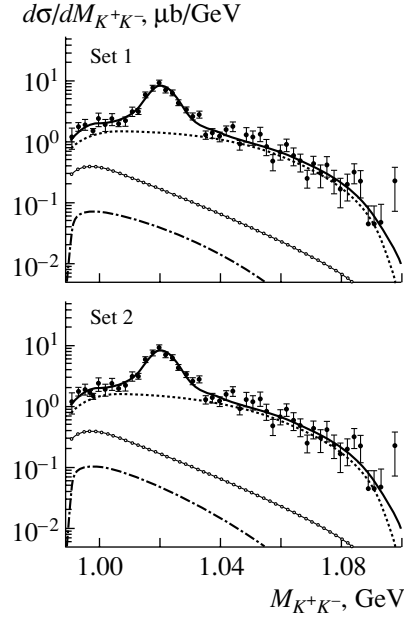


Fig. 8. The K^+K^- invariant mass distribution for the $pp \rightarrow ppK^+K^-$ reaction at $p_{\text{lab}} = 3.67$ GeV/ c . The dotted curves indicate the 4-body phase space with constant interaction amplitude, the dash-dotted curves show the coherent sum of $s(N)$ and $u(N)$ channels with interference. The solid curves with open circles correspond to the f_0 contribution from [41]. The thick solid curves show the sum of all contributions including the decay $\phi \rightarrow K^+K^-$. The experimental data are taken from [50].

with $\Lambda_N = 1.35$ GeV, respectively. We mention that the latter (dipole) result is in better agreement with the constraints on the near-threshold production of a_0 in the reaction $\pi^+ p \rightarrow K^+\bar{K}_0^0 p$ (see Section 3). In the middle part of Fig. 7, the solid curves with full dots and with open squares present the results within the ρ_2 and ρ_2, b_1 Regge exchange model. The dotted curve shows the 4-body phase space (with constant interaction amplitude), while the dashed curve is the parametrization from Sibirtsev *et al.* [39]. We note, that the cross sections for parameter set 2 (9) are similar to set 1 (8) and larger by a factor of about 1.5.

In the lower part of Fig. 7, we show the calculated total cross section (within parameter set 1) for the reaction $pp \rightarrow ppa_0^+ \rightarrow ppK^+K^-$ as a function of $Q = \sqrt{s} - \sqrt{s_0}$ in comparison to the experimental data. The closed circles indicate the data for $pp \rightarrow ppK^0\bar{K}_0^0$ from [38], the open square for $pp \rightarrow ppK^+K^-$ is from the DISTO collaboration [50], and the closed triangles show the data from COSY-11 [51].

For the $pp \rightarrow ppa_0^+ \rightarrow ppK^+K^-$ reaction (as for $pp \rightarrow ppa_0^0$), there is no contribution from meson Regge trajectories; s and u channels give similar contributions such that their interference according to the effective OPE model (curve $s + u + \text{int.}$) is

strongly destructive (cf. upper part of Fig. 6). The $t(f_1)$ contribution (dotted curve) is practically negligible, while the $t(\eta)$ channel (rare-dotted curve) becomes important closer to the threshold.

Thus, our model gives quite small cross sections for a_0^0 production in the $pp \rightarrow ppK^+K^-$ reaction, which complicates its experimental observation for this isospin channel. The situation looks more promising for the $pp \rightarrow pna_0^+ \rightarrow pnK^+\bar{K}^0$ reaction since the a_0^+ -production cross section is an order of magnitude larger than the a_0^0 one. Moreover, as has been pointed out with respect to Fig. 6, the influence of the interference is not as strong as that for the $pp \rightarrow pp a_0^0 \rightarrow ppK^+K^-$ reaction.

Here, we stress again the limited applicability of the ELM at high energies. As seen from the upper part of Fig. 7, the ELM calculations at high energies go through the experimental data, which is not realistic since other channels also contribute to $K^+\bar{K}^0$ production in pp reactions (cf. dashed curve from [39], Fig. 7, middle part). Moreover, the ELM calculations are higher than the Regge model predictions, which indicates that the ELM amplitudes at high energies have to be Reggeized.

4.2.2. Numerical results for the invariant mass distribution. As follows from the lower part of Fig. 7, the a_0 contribution to the K^+K^- production in the $pp \rightarrow ppK^+K^-$ reaction near the threshold is hardly seen. With increasing energy, the cross section grows; however, even at $Q = 0.111$ GeV, the full cross section with interference ($s + u + \text{int.}$) gives only a few percent contribution to the $0.11 \pm 0.009 \pm 0.046 \mu\text{b}$ “nonresonant” cross section (without $\phi \rightarrow K^+K^-$) from the DISTO collaboration [50].

To clarify the situation with the relative contribution of a_0^0 to the total K^+K^- production in pp reactions, we calculate the K^+K^- invariant mass distribution for the $pp \rightarrow ppK^+K^-$ reaction at $p_{\text{lab}} = 3.67$ GeV/ c , which corresponds to the kinematical conditions for the DISTO experiment [50]. The differential results are presented in Fig. 8. The upper part shows the calculation within parameter set 1, whereas the lower part corresponds to set 2. The dash-dotted curves indicate the coherent sum of $s(N)$ and $u(N)$ channels with interference for the a_0 contribution. However, one has to consider also the contribution from the f_0 scalar meson, i.e., the $pp \rightarrow pp f_0 \rightarrow ppK^+K^-$ reaction. The f_0 production in pp reactions has been studied in detail in [41]. Here, we use the result from [41] and show in Fig. 8 the contribution from the f_0 meson (calculated with parameter set A from [41]) as the solid curve with open circles.

We find that, when adding the f_0 contribution to the phase space of nonresonant K^+K^- production

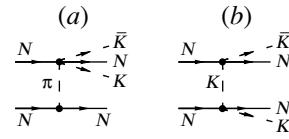


Fig. 9. Diagrams describing different mechanisms of nonresonant $K\bar{K}$ production in the reaction $NN \rightarrow NNK\bar{K}$.

(the dotted curves in Fig. 8) and the contribution from ϕ decays (resonance peak around 1.02 GeV), the sum (thick solid) curves almost perfectly describe the DISTO data. This means that there is no visible signal for an a_0^0 contribution in the DISTO data according to our calculations, while the f_0 meson gives some contribution to the K^+K^- invariant mass distribution at low invariant masses M , that is, about 12% of the total “nonresonant” cross section from the DISTO collaboration [50]. Thus, the reaction $pp \rightarrow pnK^+\bar{K}^0$ is more promising for a_0 measurements, as has been pointed out above.

4.2.3. Nonresonant background. Following [39], we consider two mechanisms of nonresonant $K\bar{K}$ production, related to pion and kaon exchanges, which are described by the diagrams in Fig. 9. The pion-exchange amplitude can be calculated using the results of Section 3. As concerning the kaon-exchange mechanism, the amplitude of the reaction $NN \rightarrow NN a_0 \rightarrow NNK\bar{K}$ can be written as

$$M_{K\text{-exch}}(p_a, p_b; p_c, p_d, k_1, k_2) \quad (32)$$

$$= \frac{F_K^2(q^2)}{q^2 - m_K^2} \bar{u}(p_c) A_{KN \rightarrow KN}(p_c, k_1; p_a, q) u(p_a)$$

$$\times \bar{u}(p_d) A_{\bar{K}N \rightarrow \bar{K}N}(p_d, k_2; p_b, q) u(p_b)$$

with permutations of nucleons in the initial and final states. Here, p_a, p_b and p_c, p_d are the 4-momenta of the initial and final nucleons, respectively; k_1 and k_2 are the momenta of the final kaons; q is the momentum of the virtual kaon; and $F_K(q^2)$ is the kaon form factor, which we take in the monopole form with the cutoff parameter $\Lambda = 1.2$ GeV.

The antikaon–nucleon amplitude $A_{\bar{K}N \rightarrow \bar{K}N}$ has been taken from [52] explicitly. Since near threshold the $KN \rightarrow KN$ cross section depends mainly on the normalization of the amplitude, but not on its spin dependence, we adopt the simplest approximation that the amplitude $A_{KN \rightarrow KN}$ is a Lorentz scalar. This allows us to connect the $A_{KN \rightarrow KN}$ amplitude (squared) by simple kinematical factor to the $KN \rightarrow KN$ cross section, where the parametrization for the elastic $K^+p \rightarrow K^+p$ cross section has been taken from [53] and the $K^0p \rightarrow K^+n$ cross section has been parametrized according to the existing data [38, 54].

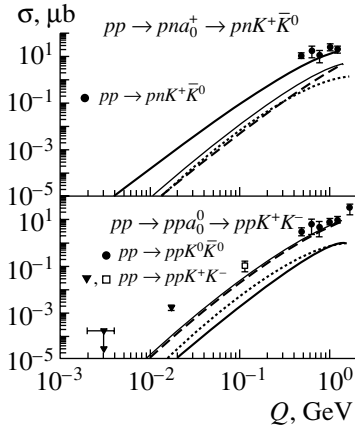


Fig. 10. Comparison of the a_0 -resonance contribution (thick solid curves) and nonresonant background (thin solid curves) in the reactions $pp \rightarrow pnK^+\bar{K}^0$ and $pp \rightarrow ppK^+K^-$. The contribution of the pion-exchange mechanism is shown by the dotted curves, and the dashed curves describe the K -exchange mechanism. The thin solid curves show the sum of the pion- and kaon-exchange mechanisms. The experimental data are taken from [50].

The results of our calculations are shown in Fig. 10 in comparison to the experimental data. The contribution of the pion-exchange mechanism is shown by the dotted curves. The dashed curves describe the K -exchange mechanism. The thin solid curves show the total background, which in our model is the sum of pion- and kaon-exchange contribution. This background can be compared with the a_0 -production cross section shown by the thick solid curves. In the case of the reaction $pp \rightarrow pnK^+\bar{K}^0$ (upper part), the a_0 -production cross section is much larger than the background, while, in the case of the reaction $pp \rightarrow ppK^+K^-$ (lower part), the $a_0(980)$ -resonance contribution appears to be much smaller than the nonresonant background. We mention that the disagreement with the DISTO ($Q \simeq 100$ MeV) and COSY-11 ($Q \simeq 17$ MeV) data should be related to the K^-pp FSI, which is known to be strong.

4.2.4. Concluding remarks on a_0 production in pN reactions. In this section, we have estimated the cross sections of a_0 production in the reactions $pp \rightarrow ppa_0^0$ and $pp \rightarrow pna_0^+$ near the threshold and at medium energies. Using an effective Lagrangian approach with OPE, we have analyzed different contributions to the cross section corresponding to t -channel diagrams with $\eta(550)$ - and $f_1(1285)$ -meson exchanges as well as s - and u -channel graphs with an intermediate nucleon. We additionally have considered the t -channel Reggeon exchange mechanism with parameters normalized to the Brookhaven data for $\pi^-p \rightarrow a_0^-p$ at 18 GeV/ c

[35]. These results have been used to calculate the contribution of a_0 mesons to the cross sections of the reactions $pp \rightarrow pnK^+\bar{K}^0$ and $pp \rightarrow ppK^+K^-$. Due to unfavorable isospin Clebsh–Gordan coefficients as well as rather strong destructive interference of the s - and u -channel contributions, our model gives quite small cross sections for a_0^0 production in the $pp \rightarrow ppK^+K^-$ reaction. However, the a_0^+ -production cross section in the $pp \rightarrow pna_0^+ \rightarrow pnK^+\bar{K}^0$ reaction should be larger by about an order of magnitude. Therefore, the experimental observation of a_0^+ in the reaction $pp \rightarrow pnK^+\bar{K}^0$ is much more promising than the observation of a_0^0 in the reaction $pp \rightarrow ppK^+K^-$. We note in passing that the $\pi\eta$ decay channel is experimentally more challenging since, due to the larger nonresonant background [55], the identification of the η meson (via its decay into photons) in a neutral-particle detector is required.

We have also analyzed invariant mass distributions of the $K\bar{K}$ system in the reaction $pp \rightarrow pNa_0 \rightarrow pNK\bar{K}$ at different excess energies Q not far from the threshold. Our analysis of the DISTO data on the reaction $pp \rightarrow ppK^+K^-$ at 3.67 GeV/ c has shown that the a_0^0 meson is hardly seen in $d\sigma/dM$ at low invariant masses; however, the f_0 meson gives some visible contribution. In this respect, the possibility of measuring the a_0^+ meson in $d\sigma/dM$ for the reaction $pp \rightarrow pnK^+\bar{K}^0$ (or $\rightarrow dK^+\bar{K}^0$) looks much more promising not only due to a much larger contribution for the a_0^+ , but also due to the absence of the f_0 meson in this channel. It is also very important that the nonresonant background is expected to be much smaller than the a_0 signal in the $pp \rightarrow pnK^+\bar{K}^0$ reaction.

Experimental data on a_0 production in NN collisions are practically absent (except for the a_0 observation in the reaction $pp \rightarrow dX$ [49]). Such measurements might give new information on the a_0 structure. According to Atkinson *et al.* [56], a relatively strong production of a_0 [the same as for the $b_1(1235)$] in nondiffractive reactions can be considered as evidence for a $q\bar{q}$ state rather than a $qq\bar{q}\bar{q}$ state. For example, the cross section of a_0 production in γp reactions at 25–50 GeV is about 1/6 of the cross sections for ρ and ω production. Similar ratios are found in the two-body reaction $pp \rightarrow dX$ at 3.8–6.3 GeV/ c , where $\sigma(pp \rightarrow da_0^+) = (1/4 - 1/6)\sigma(pp \rightarrow d\rho^+)$.

In our case, we can compare a_0 and ω production. Our model predicts $\sigma(pp \rightarrow pna_0^+) = 30\text{--}70 \mu\text{b}$ at $Q \simeq 1$ GeV, which can be compared with $\sigma(pp \rightarrow pp\omega) \simeq 100\text{--}200 \mu\text{b}$ at the same Q . If such a large cross section could be detected experimentally, this would be a serious argument in favor of the $q\bar{q}$ model for a_0 .

To distinguish between the threshold cusp scenario and a resonance model, one can exploit different analytical properties of the a_0 -production amplitudes. In case of a genuine resonance, the amplitude of $\eta\pi$ and $K\bar{K}$ production through a_0 has a pole and satisfies the factorization property. This implies that the shapes of the invariant mass distributions in the $\eta\pi$ and $K\bar{K}$ channels should not depend on the specific reaction in which a_0 resonance is produced (for $Q \geq \Gamma_{\text{tot}}$). On the other hand, for the threshold cusp scenario, the a_0 bump is produced through the $\pi\eta$ FSI. The corresponding amplitude has a square root singularity and in general cannot be factorized (see, e.g., [46], where the factorization property was disproven for pp FSI in the reaction $pp \rightarrow ppM$). This implies that, for a threshold bump, the invariant mass distributions in the $\eta\pi$ and $K\bar{K}$ channels are expected to be different for different reactions and will depend on kinematical conditions (i.e., momentum transfer) even at the same value of excess energy, e.g., $Q \simeq 1$ GeV.

5. $a_0(980)$ - $f_0(980)$ MIXING AND ISOSPIN VIOLATION IN THE REACTIONS $pN \rightarrow da_0$, $pd \rightarrow {}^3\text{He}({}^3\text{H})a_0$, AND $dd \rightarrow {}^4\text{He}a_0$

5.1. Hints for $a_0(980)$ - $f_0(980)$ Mixing

As was suggested long ago in [11], the dynamical interaction of the $a_0(980)$ and $f_0(980)$ mesons with states close to the $K\bar{K}$ threshold may give rise to a significant $a_0(980)$ - $f_0(980)$ mixing. Different aspects of this mixing and the underlying dynamics, as well as the possibilities of measuring this effect, have been discussed in [3, 12–17]. Furthermore, it has been suggested by Close and Kirk [16] that the new data from the WA102 collaboration at CERN [26] on the central production of f_0 and a_0 in the reaction $pp \rightarrow p_s X p_f$ provide evidence for a significant f_0 - a_0 -mixing intensity as large as $|\xi|^2 = (8 \pm 3)\%$. In this section, we will discuss possible experimental tests of this mixing in the reactions

$$\begin{aligned} pp &\rightarrow da_0^+ \quad (\text{a}), & pn &\rightarrow da_0^0 \quad (\text{b}), \\ pd &\rightarrow {}^3\text{H}a_0^+ \quad (\text{c}), & pd &\rightarrow {}^3\text{He}a_0^0 \quad (\text{d}), \\ dd &\rightarrow {}^4\text{He}a_0^0 \quad (\text{e}) \end{aligned}$$

near the corresponding thresholds. We recall that the a_0 meson can decay to $\pi\eta$ or $K\bar{K}$. Here, we only consider the dominant $\pi\eta$ -decay mode. Note that the isospin-violating anisotropy in reaction (b) due to the $a_0(980)$ - $f_0(980)$ mixing is very similar to that which might arise in the reaction $pn \rightarrow d\pi^0$ because of the π^0 - η mixing (see [57]). Recently, measurements of the charge-symmetry breaking in the

reactions $\pi^+d \rightarrow pp\eta$ and $\pi^-d \rightarrow nn\eta$ near the η -production threshold were performed at BNL [57]. A similar experiment, comparing the reactions $pd \rightarrow {}^3\text{He}\pi^0$ and $pd \rightarrow {}^3\text{H}\pi^+$ near the η -production threshold, is now being performed at COSY (Jülich) (see, e.g., [58]).

5.2. Reactions $pp \rightarrow da_0^+$ and $pn \rightarrow da_0^0$

5.2.1. Phenomenology of isospin violation.

In reactions (a) and (b), the final da_0 system has isospin $I_f = 1$; for $l_f = 0$ (S -wave production close to threshold), it has spin-parity $J_f^P = 1^+$. The initial NN system cannot be in the state $I_i = 1$, $J_i^P = 1^+$ due to the Pauli principle. Therefore, near threshold, the da_0 system should be dominantly produced in the P wave with quantum numbers $J_f^P = 0^-, 1^-,$ or 2^- . The states with $J_i^P = 0^-, 1^-,$ or 2^- can be formed by an NN system with spin $S_i = 1$ and $l_i = 1$ and 3. At the beginning, for qualitative discussion, we neglect the contribution of the higher partial wave ($l_i = 3$).⁵⁾ In this case, we can write the amplitude of reaction (a) in the following form:

$$\begin{aligned} T(pn \rightarrow da_0^+) &= \alpha^+(\mathbf{p} \cdot \mathbf{S})(\mathbf{k} \cdot \mathbf{e}^*) \quad (33) \\ &+ \beta^+(\mathbf{p} \cdot \mathbf{k})(\mathbf{S} \cdot \mathbf{e}^*) + \gamma^+(\mathbf{S} \cdot \mathbf{k})(\mathbf{p} \cdot \mathbf{e}^*), \end{aligned}$$

where $\mathbf{S} = \phi_N^T \sigma_2 \sigma \phi_N$ is the spin operator of the initial NN system; \mathbf{p} and \mathbf{k} are the initial and final c.m. momenta; \mathbf{e} is the deuteron polarization vector; and α^+ , β^+ , and γ^+ are three independent scalar amplitudes that can be considered as constants near threshold (at $k \rightarrow 0$).

Due to the mixing, a_0^0 may also be produced via f_0 . In this case, the a_0^0d system will be in the S wave and the amplitude of reaction (b) can be written as

$$\begin{aligned} T(pn \rightarrow da_0^0) &= \alpha^0(\mathbf{p} \cdot \mathbf{S})(\mathbf{k} \cdot \mathbf{e}^*) \quad (34) \\ &+ \beta^0(\mathbf{p} \cdot \mathbf{k})(\mathbf{S} \cdot \mathbf{e}^*) + \gamma^0(\mathbf{S} \cdot \mathbf{k})(\mathbf{p} \cdot \mathbf{e}^*) + \xi F(\mathbf{S} \cdot \mathbf{e}^*), \end{aligned}$$

where ξ is the mixing parameter and F is the f_0 production amplitude. In the limit $k \rightarrow 0$, F is again a constant. The scalar amplitudes α , β , and γ for reactions (a) and (b) are related to each other by a relative factor of $\sqrt{2}$ as $\alpha^+ = \sqrt{2}\alpha^0$, $\beta^+ = \sqrt{2}\beta^0$, and $\gamma^+ = \sqrt{2}\gamma^0$.

The differential cross sections for reactions (a) and (b) have the form (up to terms linear in ξ)

$$\frac{d\sigma(pp \rightarrow da_0^+)}{d\Omega} = 2 \frac{k}{p} (C_0 + C_2 \cos^2 \theta), \quad (35)$$

⁵⁾See, e.g., phenomenological analysis in [59], where this partial wave was also taken into account.

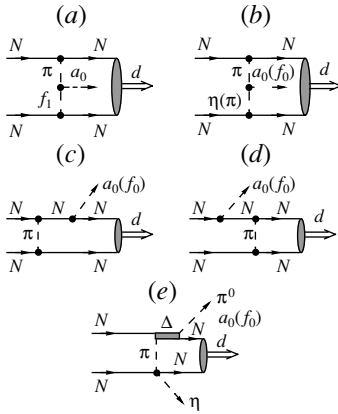


Fig. 11. Diagrams describing (a–d) different mechanisms of a_0 - and f_0 -meson production in the reaction $NN \rightarrow da_0(f_0)$ within the framework of the TSM and (e) the nonresonant $\pi\eta$ production.

$$\frac{d\sigma(pn \rightarrow da_0^0)}{d\Omega} = \frac{k}{p} (C_0 + C_2 \cos^2 \theta + C_1 \cos \theta), \quad (36)$$

where

$$\begin{aligned} C_0 &= \frac{1}{2} p^2 k^2 [|\alpha^0|^2 + |\gamma^0|^2], \\ C_1 &= pk \operatorname{Re}((\xi F)^* (\alpha^0 + 3\beta^0 + \gamma^0)), \\ C_2 &= \frac{1}{2} p^2 k^2 [3|\beta^0|^2 \\ &\quad + 2\operatorname{Re}(\alpha^0 \beta^{0*} + \alpha^0 \gamma^{0*} + \beta^0 \gamma^{0*})]. \end{aligned} \quad (37)$$

Similarly, the differential cross section of the reaction $pn \rightarrow df_0$ can be written as

$$\frac{d\sigma(pn \rightarrow df_0)}{d\Omega} = \frac{3k}{2p} |F|^2. \quad (38)$$

The mixing effect—described by the term $C_1 \cos \theta$ in Eq. (36)—then leads to an isospin violation in the ratio R_{ba} of the differential cross sections for reactions (b) and (a),

$$R_{ba} = \frac{1}{2} + \frac{1}{2} \frac{C_1 \cos \theta}{C_0 + C_2 \cos^2 \theta}, \quad (39)$$

and to the forward–backward asymmetry for reaction (b),

$$A_b(\theta) = \frac{\sigma_b(\theta) - \sigma_b(\pi - \theta)}{\sigma_b(\theta) + \sigma_b(\pi - \theta)} = \frac{C_1 \cos \theta}{C_0 + C_2 \cos^2 \theta}. \quad (40)$$

The latter effect has been already discussed in [60], where it was argued that the asymmetry $A_b(\theta = 0)$ can reach 5–10% at an energy excess of $Q = 5$ –10 MeV. However, if we adopt a mixing parameter $|\xi|^2 = (8 \pm 3)\%$, as follows from the WA102 data, we can expect a much larger asymmetry. We note

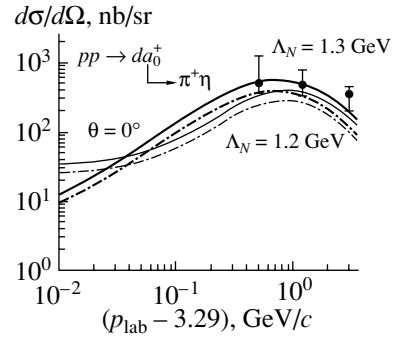


Fig. 12. Forward differential cross section of the reaction $pp \rightarrow da_0^+$ as a function of $(p_{\text{lab}} - 3.29) \text{ GeV}/c$. The dots are the experimental data from [49], while the thick dash-dotted and solid curves describe the results of the TSM for $\Lambda_N = 1.2$ and 1.3 GeV , respectively. The thin curves are calculated using the Flatté mass distribution for the a_0 meson with a cut $M_{\pi+\eta} \geq 0.85 \text{ GeV}$ and $\Lambda_N = 1.2 \text{ GeV}$ (dash-dotted curve) or 1.3 GeV (solid curve).

explicitly that the coefficient C_1 in (37) depends not only on the magnitude of the mixing parameter ξ , but also on the relative phases with respect to the amplitudes of f_0 and a_0 production, which are unknown so far. This uncertainty has to be kept in mind for the following discussion.

If a_0 and f_0 were very narrow particles, then near threshold the differential cross section (35), dominated by the P wave, would be proportional to k^3 or $Q^{3/2}$, where Q is the c.m. energy excess. Due to S -wave dominance in the reaction $pn \rightarrow df_0$, one would expect that the cross section scales like $\sim k$ or $\sim \sqrt{Q}$. In this limit, the a_0 – f_0 mixing leads to an enhancement of the asymmetry $A_b(\theta)$ as $1/k$ near the threshold. In reality, however, both a_0 and f_0 have widths of about 40–100 MeV. Therefore, at fixed initial momentum, their production cross section should be averaged over the corresponding mass distributions. This will essentially change the threshold behavior of the cross sections. Another complication is that broad resonances are usually accompanied by background lying underneath the resonance signals. These problems will be discussed below in the following subsections.

5.2.2. Model calculations. In order to estimate isospin-violation effects in the differential cross-section ratio R_{ba} and in the forward–backward asymmetry A_b , we use the two-step model (TSM), which was successfully applied earlier to the description of η -, η' -, ω -, and ϕ -meson production in the reaction $pN \rightarrow dX$ in [61, 62]. Recently, this model has been also used for an analysis of the reaction $pp \rightarrow da_0^+$ [18].

The diagrams in Fig. 11 describe the different mechanisms of a_0 - and f_0 -meson production in the

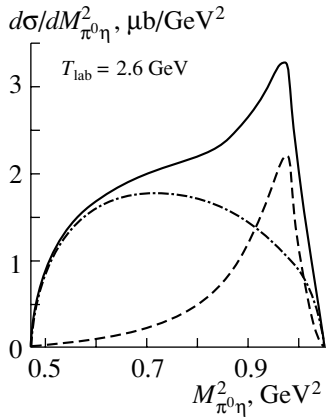


Fig. 13. $\pi^0\eta$ Invariant mass distribution for the reaction $pn \rightarrow d\pi^0\eta$ at 3.4 GeV/c. The dashed and dash-dotted curves describe the a_0 resonance contribution and non-resonance background, respectively; the solid curve is the sum of both contributions.

reaction $NN \rightarrow da_0(f_0)$ within the framework of the TSM. In the case of a_0 production, the amplitude of the subprocess $\pi N \rightarrow a_0 N$ contains three different contributions: (i) the $f_1(1285)$ -meson exchange (Fig. 11a), (ii) the η -meson exchange (Fig. 11b), and (iii) s - and u -channel nucleon exchanges (Figs. 11c and 11d). As it was shown in [18], the main contribution to the cross section for the reaction $pp \rightarrow da_0^+$ stems from the u -channel nucleon exchange (i.e., from the diagram of Fig. 11d) and all other contributions can be neglected. In order to preserve the correct structure of the amplitude under permutations of the initial nucleons (which is antisymmetric for the isovector state and symmetric for the isoscalar state), the amplitudes of a_0 and f_0 production can be written as the following combinations of the t - and u -channel contributions:

$$T_{pn \rightarrow da_0^0}(s, t, u) = A_{pn \rightarrow da_0^0}(s, t) - A_{pn \rightarrow da_0^0}(s, u), \quad (41)$$

$$T_{pn \rightarrow df_0}(s, t, u) = A_{pn \rightarrow df_0}(s, t) + A_{pn \rightarrow df_0}(s, u),$$

where $s = (p_1 + p_2)^2$; $t = (p_3 - p_1)^2$; $u = (p_3 - p_2)^2$; and p_1, p_2, p_3 , and p_4 are the 4-momenta of the initial protons, meson M , and the deuteron, respectively. The structure of the amplitudes (41) guarantees that the S -wave part vanishes in the case of direct a_0 production since it is forbidden by angular momentum conservation and the Pauli principle. Also, higher partial waves are included in (41) (in contrast to the simplified discussion in Subsection 5.1).

In the case of f_0 production, the amplitude of the subprocess $\pi N \rightarrow f_0 N$ contains two different contributions: (i) the π -meson exchange (Fig. 11b) and (ii) s - and u -channel nucleon exchanges (Figs. 11c and 11d). Our analysis has shown that, similar to the

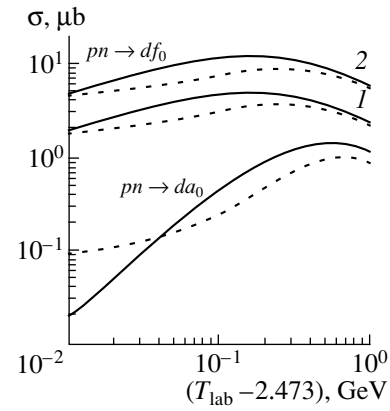


Fig. 14. Total cross sections for the reactions $pn \rightarrow da_0$ and $pn \rightarrow df_0$ as functions of $(T_{\text{lab}} - 2.473)$ GeV. The solid and dashed curves are calculated using narrow and finite resonance widths, respectively. The curves denoted by 1 and 2 correspond to the choices $R(f_0/a_0) = 1.46$ and 2.3, respectively.

case of a_0 production, the main contribution to the cross section of the reaction $pn \rightarrow df_0$ is due to the u -channel nucleon exchange (i.e., from the diagram of Fig. 11d); the contribution of the combined $\pi\pi$ exchange (Fig. 11b) as well as the s -channel nucleon exchange can be neglected. In this case, we get for the ratio of the squared amplitudes

$$\frac{|A_{pn \rightarrow df_0}(s, t)|^2}{|A_{pn \rightarrow da_0}(s, t)|^2} = \frac{|A_{pn \rightarrow df_0}(s, u)|^2}{|A_{pn \rightarrow da_0}(s, u)|^2} = \frac{|g_{f_0 NN}|^2}{|g_{a_0 NN}|^2}. \quad (42)$$

If we take $g_{a_0 NN} = 3.7$ (see, e.g., [27]) and $g_{f_0 NN} = 8.5$ [28], then we find for the ratio of the amplitudes $R(f_0/a_0) = g_{f_0 NN}/g_{a_0 NN} = 2.3$. Note, however, that Mull and Holinde [28] give a different value for the ratio of the coupling constants $R(f_0/a_0) = 1.46$, which is lower by about 37%. In the following, we use $R(f_0/a_0) = 1.46-2.3$.

The forward differential cross section for reaction (a) as a function of the proton beam momentum is presented in Fig. 12. The thick dash-dotted and solid curves (taken from [18] and calculated for the zero width limit) describe the results of the TSM for different values of the nucleon cutoff parameter, $\Lambda_N = 1.2$ and 1.3 GeV, respectively.

In order to take into account the finite width of a_0 , we use a Flatté mass distribution with the same parameters as in [19]: the K -matrix pole at 999 MeV, $\Gamma_{a_0 \rightarrow \pi\eta} = 70$ MeV, and $\Gamma(K\bar{K})/\Gamma(\pi\eta) = 0.23$ (see also [24] and references therein). The thin dash-dotted and solid curves in Fig. 12 are calculated within TSM using this mass distribution with the cut $M_{\pi+\eta} \geq 0.85$ GeV and $\Lambda_N = 1.2$ and 1.3 GeV, respectively. The corresponding $\pi^0\eta$ invariant mass

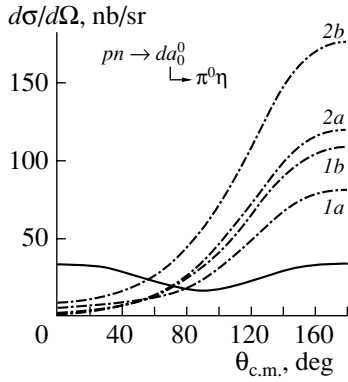


Fig. 15. Differential cross section of the reaction $pn \rightarrow da_0^0$ at $T_{\text{lab}} = 2.6$ GeV as a function of $\theta_{\text{c.m.}}$. The solid curve corresponds to the case of isospin conservation, i.e., $|\xi|^2 = 0$. The dash-dotted curves include the mixing effect with $|\xi|^2 = 0.05$ for the lower curves (*1a* and *2a*) and $|\xi|^2 = 0.11$ for the upper curves (*1b* and *2b*). The curves *1a*, *1b* and *2a*, *2b* have been calculated for $R(f_0/a_0) = 1.46$ and 2.3 , respectively.

distribution for the reaction $pn \rightarrow da_0^0 \rightarrow d\pi^0\eta$ at 3.4 GeV/ c is shown in Fig. 13 by the dashed curve.

In the case of the f_0 meson, where $\text{Br}(K\bar{K})$ is not yet fixed [24], we use the Breit–Wigner mass distribution with $M_R = 980$ MeV and $\Gamma_R \simeq \Gamma_{f_0 \rightarrow \pi\pi} = 70$ MeV.

The calculated total cross sections for the reactions $pn \rightarrow da_0$ and $pn \rightarrow df_0$ (as a function of T_{lab} for $\Lambda_N = 1.2$ GeV) are shown in Fig. 14. The solid and dashed curves describe the calculations with zero and finite widths, respectively. In the case of f_0 production in the $\pi\pi$ mode, we take the same cut in the invariant mass of the $\pi\pi$ system, $M_{\pi\pi} \geq 0.85$ GeV. The curves denoted by *1* and *2* are obtained for $R(f_0/a_0) = 1.46$ and 2.3 . Comparing the solid and dashed curves, we see that near the threshold the finite-width corrections to the cross sections are quite important. The most important changes are introduced to the energy behavior of the a_0 -production cross section. (Compare also thick and thin curves in Fig. 12.)

In principle, mixing can modify the mass spectrum of the a_0 and f_0 . However, in this case, the effect is expected to be less spectacular than for the ρ - ω case where the widths of ρ and ω are very different (see, e.g., the discussion in [57] and references therein). Nevertheless, the modification of the a_0^0 spectral function due to a_0 - f_0 mixing can be measured comparing the invariant mass distributions of a_0^0 with that of a_0^+ . According to our analysis, a much cleaner signal for isospin violation can be obtained from the measurement of the forward–backward asymmetry in the reaction $pn \rightarrow da_0^0 \rightarrow d\pi^0\eta$ for the integrated strength of the a_0 . That is why, for all calculations

on isospin-violation effects below, the strengths of f_0 and a_0 are integrated over the invariant masses in the interval 0.85 – 1.02 GeV.

The magnitude of the isospin-violation effects is shown in Fig. 15, where we present the differential cross section of the reaction $pn \rightarrow da_0^0$ at $T_{\text{lab}} = 2.6$ GeV as a function of $\theta_{\text{c.m.}}$ for different values of the mixing intensity $|\xi|^2 = 0.05$ and 0.11 . For reference, the solid curve shows the case of isospin conservation, i.e., $|\xi|^2 = 0$. The dash-dotted curves include the mixing effect. Note that all curves in Fig. 15 were calculated assuming maximal interference of the amplitudes describing the direct a_0 production and its production through f_0 . The maximal values of the differential cross section may also occur at $\theta_{\text{c.m.}} = 0^\circ$ depending on the sign of the coefficient C_1 in Eq. (36).

It follows from Fig. 15 in either case that the isospin-violation parameter $A_b(\theta)$ for $\theta_{\text{c.m.}} = 180^\circ$ may be quite large, i.e.,

$$A_b(180^\circ) = 0.86 - 0.96 \text{ or } 0.9 - 0.98 \quad (43)$$

for $R(f_0/a_0) = 1.46$ or 2.3 , respectively. Note that the asymmetry depends rather weakly on $R(f_0/a_0)$. It might be more sensitive to the relative phase of a_0 and f_0 contributions.

5.2.3. Background. The dash-dotted curve in Fig. 13 shows our estimates of possible background from nonresonant $\pi^0\eta$ production in the reaction $pn \rightarrow d\pi^0\eta$ at $T_{\text{lab}} = 2.6$ GeV (see also [63]). The background amplitude was described by the diagram shown in Fig. 11e, where η and π mesons are created through the intermediate production of $\Delta(1232)$ (in the amplitude $\pi N \rightarrow \pi N$) and $N(1535)$ (in the amplitude $\pi N \rightarrow \eta N$). The total cross section of the nonresonant $\pi\eta$ production due to this mechanism was found to be $\sigma_{\text{bg}} \simeq 0.8$ μb for a cutoff in the OPE $\Lambda_\pi = 1$ GeV.

The background is charge-symmetric and cancels in the difference of the cross sections $\sigma(\theta) - \sigma(\pi - \theta)$. Therefore, the complete separation of the background is not crucial for a test of isospin violation due to the a_0 - f_0 mixing. There will also be some contribution from π - η mixing as discussed in [57, 58]. According to the results of [57], this mechanism yields a charge-symmetry breaking in the ηNN system of about 6%:

$$R = d\sigma(\pi^+d \rightarrow pp\eta)/d\sigma(\pi^-d \rightarrow nn\eta) = 0.938 \pm 0.009.$$

A similar isospin violation due to π - η mixing can also be expected in our case.

The best strategy to search for isospin violation is a measurement of the forward–backward asymmetry for different intervals of $M_{\pi^0\eta}$. As follows from Fig. 13, we have $\sigma_{a_0}(\sigma_{\text{bg}}) = 0.3(0.4)$, $0.27(0.29)$, and

0.19(0.15) μb for $M_{\pi^0\eta} \geq 0.85, 0.9,$ and 0.95 GeV, respectively. For $M_{\pi^0\eta} \leq 0.7$ GeV, the resonance contribution is rather small and the charge-symmetry breaking will be mainly related to $\pi-\eta$ mixing and, therefore, will be small. On the other hand, in the interval $M_{\pi^0\eta} \geq 0.95$ GeV, the background does not exceed the resonance contribution and we expect a comparatively large isospin breaking due to a_0-f_0 mixing.

5.3. Reaction $pn \rightarrow df_0 \rightarrow d\pi\pi$

The isospin-violation effects can also be measured in the reaction

$$pn \rightarrow df_0 \rightarrow d\pi^+\pi^-, \quad (44)$$

where, due to mixing, the f_0 may also be produced via the a_0 . The corresponding differential cross section is shown in Fig. 16. The differential cross section for f_0 production is expected to be substantially larger than for a_0 production, but the isospin-violation effect turns out to be smaller than in the $\pi\eta$ -production channel. Nevertheless, the isospin-violation parameter A is expected to be about 10–30% and can be detected experimentally.

5.4. Reactions $pd \rightarrow {}^3\text{H} a_0^+$ and $pd \rightarrow {}^3\text{He} a_0^0$

We continue with pd reactions and compare the final states ${}^3\text{H} a_0^+$ (c) and ${}^3\text{He} a_0^0$ (d). Near the threshold, the amplitudes of these reactions can be written as

$$T(pd \rightarrow {}^3\text{H} a_0^+) = \sqrt{2} D_a \mathbf{S}_A \cdot \mathbf{e}, \quad (45)$$

$$T(pd \rightarrow {}^3\text{He} a_0^0) = (D_a + \xi D_f) \mathbf{S}_A \cdot \mathbf{e}, \quad (46)$$

with $\mathbf{S}_A = \phi_A^T \sigma_2 \sigma \phi_N$. D_a and D_f are the scalar S -wave amplitudes describing the a_0 and f_0 production in the case of $\xi = 0$. The ratio of the differential cross sections for reactions (d) and (c) is then given by

$$R_{\text{dc}} = \frac{|D_a + \xi D_f|^2}{2|D_a|^2} = \frac{1}{2} + \frac{2\text{Re}(D_a^* \xi D_f) + |\xi D_f|^2}{|D_a|^2}. \quad (47)$$

The magnitude of the ratio R_{dc} now depends on the relative value of the amplitudes D_a and D_f . If they are comparable ($|D_a| \sim |D_f|$) or $|D_f|^2 \gg |D_a|^2$, the deviation of R_{dc} from 0.5 (which corresponds to isospin conservation) might be 100% or more. Only in the case $|D_f|^2 \ll |D_a|^2$ will the difference of $|R_{\text{dc}}|^2$ from 0.5 be small. However, this seems to be very unlikely.

Using the two-step model for the reactions $pd \rightarrow {}^3\text{He} a_0^0$ and $pd \rightarrow {}^3\text{He} f_0$, involving the subprocesses $pp \rightarrow d\pi^+$ and $\pi^+n \rightarrow p a_0/f_0$ (cf. [64, 65]), we find

$$\frac{\sigma(pd \rightarrow {}^3\text{He} a_0^0)}{\sigma(pd \rightarrow {}^3\text{He} f_0)} \simeq \frac{\sigma(\pi^+n \rightarrow p a_0^0)}{\sigma(\pi^+n \rightarrow p f_0)}. \quad (48)$$

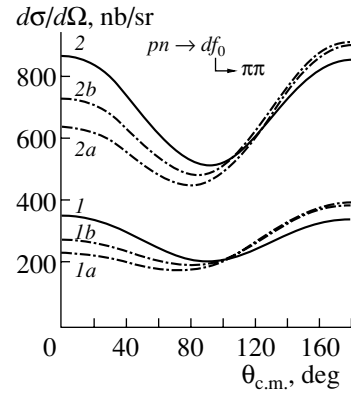


Fig. 16. Differential cross section of the reaction $pn \rightarrow df_0$ at $T_{\text{lab}} = 2.6$ GeV as a function of $\theta_{\text{c.m.}}$. The solid curves correspond to the case of isospin conservation, i.e., $|\xi|^2 = 0$. The dash-dotted curves include the mixing effect with $|\xi|^2 = 0.05$ for the lower curves ($1a$ and $2a$) and $|\xi|^2 = 0.11$ for the upper curves ($1b$ and $2b$). The curves $1, 1a, 1b$ and $2, 2a, 2b$ have been calculated for $R(f_0/a_0) = 1.46$ and 2.3 , respectively.

According to the calculations in [18], we expect $\sigma(\pi^+n \rightarrow p a_0^0) = \sigma(\pi^-p \rightarrow n a_0^0) \simeq 0.5\text{--}1$ mb at $1.75\text{--}2$ GeV/ c . A similar value for $\sigma(\pi^-p \rightarrow n f_0)$ can be found using the results from [41]. According to the latter study, $\sigma(\pi^-p \rightarrow n f_0 \rightarrow n K^+ K^-) \simeq 6\text{--}8$ μb at $1.75\text{--}2$ GeV/ c and $\text{Br}(f_0 \rightarrow K^+ K^-) \simeq 1\%$, which implies that $\sigma(\pi^-p \rightarrow n f_0) \simeq 0.6\text{--}0.8$ mb. Thus, we expect that near threshold $|D_a| \sim |D_f|$. This would imply that the effect of isospin violation in the ratio R_{dc} can become quite large.

Recently, the cross section of the reaction $pd \rightarrow {}^3\text{He} K^+ K^-$ has been measured by the MOMO collaboration at COSY (Jülich) [66]. It was found that $\sigma = 9.6 \pm 1.0$ and 17.5 ± 1.8 nb for $Q = 40$ and 56 MeV, respectively. The authors note that the invariant $K^+ K^-$ mass distributions in those data contain a broad peak which follows phase space. However, as was shown in [19], the form of the invariant mass spectrum, which follows phase space, cannot be distinguished from the a_0 -resonance contribution at such small Q . Therefore, the events from the broad peak in [66] can also be related to a_0 and/or f_0 . Moreover, due to the phase-space behavior near the threshold, one would expect a dominance of two-body reactions. Thus, the real cross section of the reaction $pd \rightarrow {}^3\text{He} a_0^0 \rightarrow {}^3\text{He} \pi^0 \eta$ is not expected to be substantially smaller than its upper limit of about $40\text{--}70$ nb at $Q = 40\text{--}60$ MeV, which follows from the MOMO data [66].

5.5. Reaction $dd \rightarrow {}^4\text{He} a_0^0$

The direct production of a_0 in the reaction $dd \rightarrow {}^4\text{He} a_0^0$ is forbidden. It thus can only be observed due

to the f_0 - a_0 mixing:

$$\frac{\sigma(dd \rightarrow {}^4\text{He} a_0^0)}{\sigma(dd \rightarrow {}^4\text{He} f_0)} = |\xi|^2. \quad (49)$$

Therefore, it will be very interesting to study the reaction

$$dd \rightarrow {}^4\text{He}(\pi^0\eta) \quad (50)$$

near the f_0 -production threshold. Any signal of the reaction (50) then will be related to isospin breaking. It is expected to be much more pronounced near the f_0 threshold as compared to the region below this threshold.

In summarizing this section, we have discussed the effects of isospin violation in the reactions $pN \rightarrow da_0$, $pn \rightarrow df_0$, $pd \rightarrow {}^3\text{He}({}^3\text{H})a_0$, and $dd \rightarrow {}^4\text{He} a_0$, which can be generated by f_0 - a_0 mixing. It has been demonstrated that, for a mixing intensity of about $(8 \pm 3)\%$, the isospin violation in the ratio of the differential cross sections of the reactions $pp \rightarrow da_0^+ \rightarrow d\pi^+\eta$ and $pn \rightarrow da_0^0 \rightarrow d\pi^0\eta$ as well as in the forward-backward asymmetry in the reaction $pn \rightarrow da_0^0 \rightarrow d\pi^0\eta$ not far from the threshold may be about 50–100%. Such large effects are caused by the interference of direct a_0 production and its production via the f_0 (the former amplitude is suppressed close to threshold due to the P -wave amplitude, whereas the latter is large due to the S -wave mechanism). A similar isospin violation is expected in the ratio of the differential cross sections of the reactions $pd \rightarrow {}^3\text{H} a_0^+(\pi^+\eta)$ and $pd \rightarrow {}^3\text{H} a_0^0(\pi^0\eta)$. Finally, we have also discussed the isospin violation effects in the reactions $pn \rightarrow df_0(\pi^+\pi^-)$ and $dd \rightarrow {}^4\text{He} a_0$. All reactions together—once studied experimentally—are expected to provide detailed information on the strength of the f_0 - a_0 mixing. Corresponding measurements are now in preparation for the ANKE spectrometer at COSY (Jülich)[67].

ACKNOWLEDGMENTS

The authors are grateful to J. Ritman for stimulating discussions and useful suggestions and to V. Baru for providing the parametrization of the FSI enhancement factor.

This work is supported by Deutsche Forschungsgemeinschaft and by the Russian Foundation for Basic Research (project no. 00-02-04025).

REFERENCES

1. F. E. Close *et al.*, Phys. Lett. B **319**, 291 (1993).
2. M. Genovese *et al.*, Nuovo Cimento A **107**, 1249 (1994).
3. G. Janssen, B. Pierce, K. Holinde, and J. Speth, Phys. Rev. D **52**, 2690 (1995).
4. V. V. Anisovich *et al.*, Phys. Lett. B **355**, 363 (1995).
5. N. A. Törnqvist, Phys. Rev. Lett. **49**, 624 (1982).
6. K. Maltman, Nucl. Phys. A **675**, 209 (2000).
7. S. Narison, Nucl. Phys. B (Proc. Suppl.) **86**, 242 (2000).
8. L. Montanet, Nucl. Phys. B (Proc. Suppl.) **86**, 381 (2000).
9. V. V. Anisovich, L. Montanet, and V. N. Nikonov, Phys. Lett. B **480**, 19 (2000).
10. S. Narison, Nucl. Phys. B (Proc. Suppl.) **96**, 244 (2001).
11. N. N. Achasov, S. A. Devyanin, and G. N. Shestakov, Phys. Lett. B **88B**, 367 (1979).
12. N. N. Achasov and G. N. Shestakov, Phys. Rev. D **56**, 212 (1997).
13. T. Barnes, Phys. Lett. B **165B**, 434 (1985).
14. O. Krehl, R. Rapp, and J. Speth, Phys. Lett. B **390**, 23 (1997).
15. B. O. Kerbikov and F. Tabakin, Phys. Rev. C **62**, 064601 (2000).
16. F. E. Close and A. Kirk, Phys. Lett. B **489**, 24 (2000).
17. V. Yu. Grishina, L. A. Kondratyuk, M. Büscher, *et al.*, Phys. Lett. B **521**, 217 (2001).
18. V. Yu. Grishina, L. A. Kondratyuk, E. L. Bratkovskaya, *et al.*, Eur. Phys. J. A **9**, 277 (2000); J. Phys. G (in print).
19. E. L. Bratkovskaya *et al.*, nucl-th/0107071.
20. V. Chernyshev *et al.*, COSY Proposal No. 55 “Study of a_0^+ Mesons at ANKE” (1997), <http://www.fz-juelich.de/ikp/anke>; L. A. Kondratyuk *et al.*, Preprint No. 18-97, ITEP (Moscow, 1997).
21. M. Büscher *et al.*, Beam-Time Request for COSY Proposal #55 “Study of a_0^+ Mesons at ANKE” (2000); <http://www.fz-juelich.de/ikp/anke>.
22. M. Büscher *et al.*, Status Report for COSY Experiment #55 “Study of a_0^+ Mesons at ANKE” and Proposal “Investigation of Neutral Scalar Mesons a_0^0/f_0 with ANKE” <http://www.fz-juelich.de/ikp/anke>
23. S. Flatté, Phys. Lett. B **63B**, 224 (1976).
24. Particle Data Group (C. Caso *et al.*), Eur. Phys. J. C **15**, 1 (2000).
25. A. Abele *et al.*, Phys. Rev. D **57**, 3860 (1998).
26. WA102 Collab. (D. Barberis *et al.*), Phys. Lett. B **440**, 225 (1998).
27. R. Machleidt, K. Holinde, and Ch. Elster, Phys. Rep. **149**, 1 (1987).
28. V. Mull and K. Holinde, Phys. Rev. C **51**, 2360 (1995).
29. M. Kirchbach and D. O. Riska, Nucl. Phys. A **594**, 419 (1995).
30. D. L. Cheshire *et al.*, Phys. Rev. Lett. **28**, 520 (1972).
31. A. B. Kaidalov, Yad. Fiz. **53**, 1410 (1991) [Sov. J. Nucl. Phys. **53**, 872 (1991)].
32. L. A. Kondratyuk *et al.*, Phys. Rev. C **48**, 2491 (1993).
33. W. D. Apel *et al.*, Yad. Fiz. **41**, 126 (1985) [Sov. J. Nucl. Phys. **41**, 80 (1985)]; D. Alde *et al.*, Phys. Lett. B **205**, 397 (1988).

34. D. Alde *et al.*, *Yad. Fiz.* **59**, 1027 (1996) [*Phys. At. Nucl.* **59**, 982 (1996)]; S. Sadovsky, in *Proceedings of the 6th International Conference on Hadron Spectroscopy "Hadron'95"*, Ed. by M. C. Birse *et al.* (World Sci., Singapore, 1996), p. 445.
35. A. R. Dzierba, in *Proceedings of the Second Workshop on Physics and Detectors for DAΦNE'95, Frascati, 1995*, Ed. by R. Baldini *et al.*, *Frascati Phys. Ser.* **4**, 99 (1996).
36. R. Kokoski and N. Isgur, *Phys. Rev. D* **35**, 907 (1987).
37. A. B. Kaidalov, *Surv. High Energy Phys.* **13**, 265 (1999).
38. *Landolt-Börnstein: Numerical Data and Functional Relationships in Science and Technology, New Series*, Ed. by H. Schopper (Springer-Verlag, Berlin, 1988), Vol. I/12.
39. A. A. Sibirtsev, W. Cassing, and C. M. Ko, *Z. Phys. A* **358**, 101 (1997).
40. O. I. Dahl *et al.*, *Phys. Rev.* **163**, 1377 (1967).
41. E. L. Bratkovskaya, W. Cassing, L. A. Kondratyuk, and A. Sibirtsev, *Eur. Phys. J. A* **4**, 165 (1999).
42. T. Hippchen, J. Haidenbauer, K. Holinde, and V. Mull, *Phys. Rev. C* **44**, 1323 (1991); V. Mull, J. Haidenbauer, T. Hippchen, and K. Holinde, *Phys. Rev. C* **44**, 1337 (1991).
43. W. S. Chung, G. Q. Li, and C. M. Ko, *Nucl. Phys. A* **625**, 371 (1997).
44. K. Nakayama, A. Szczurek, C. Hanhart, *et al.*, *Phys. Rev. C* **57**, 1580 (1998).
45. V. Baru, A. Kudryavtsev, V. Tarasov, and V. Chernyshev, Preprint No. 30-00, ITEP (Moscow, 2000).
46. V. Baru, A. M. Gasparian, J. Haidenbauer, *et al.*, *nucl-th/0006075*; *Yad. Fiz.* **64**, 633 (2001) [*Phys. At. Nucl.* **64**, 579 (2001)].
47. K. Nakayama, *nucl-th/0108032*.
48. T. Feuster and U. Mosel, *Phys. Rev. C* **58**, 457 (1998); **59**, 460 (1999).
49. M. A. Abolins *et al.*, *Phys. Rev. Lett.* **25**, 469 (1970).
50. F. Balestra *et al.*, *Phys. Rev. C* **63**, 024004 (2001).
51. C. Quentmeier *et al.*, *Phys. Lett. B* **515**, 276 (2001).
52. A. D. Martin, *Nucl. Phys. B* **179**, 33 (1981).
53. J. Cugnon, P. Deneye, and J. Vandermeulen, *Phys. Rev. C* **41**, 1701 (1990).
54. J. C. M. Armitage *et al.*, *Nucl. Phys. B* **123**, 111 (1977).
55. H. Müller, *Eur. Phys. J. A* **11**, 113 (2001).
56. M. Atkinson *et al.*, *Phys. Lett. B* **138B**, 459 (1984).
57. W. B. Tippens *et al.*, *Phys. Rev. D* **63**, 052001 (2001).
58. A. Magiera and H. Machner, *Nucl. Phys. A* **674**, 515 (2000).
59. A. Kudryavtsev *et al.*, *nucl-th/0203034*; *Phys. Rev. C* **66**, 015207 (2002).
60. A. Kudryavtsev and V. E. Tarasov, *Pis'ma Zh. Éksp. Teor. Fiz.* **72**, 589 (2000) [*JETP Lett.* **72**, 410 (2000)].
61. V. Yu. Grishina *et al.*, *Phys. Lett. B* **475**, 9 (2000).
62. V. Yu. Grishina, L. A. Kondratyuk, and M. Büscher, *Yad. Fiz.* **63**, 1913 (2000) [*Phys. At. Nucl.* **63**, 1824 (2000)].
63. V. Yu. Grishina *et al.*, in *IKP Annual Report 2000*, Berichte des Forschungszentrums Jülich, Jül-3852, ISSN 0944-2952, p. 30.
64. G. Fäldt and C. Wilkin, *Phys. Lett. B* **354**, 20 (1995).
65. L. A. Kondratyuk and Yu. N. Uzikov, *Pis'ma Zh. Éksp. Teor. Fiz.* **63**, 3 (1996) [*JETP Lett.* **63**, 1 (1996)].
66. F. Belleman *et al.*, in *IKP Annual Report 2000*, Berichte des Forschungszentrums Jülich, Jül-3852, ISSN 0944-2952, p. 62.
67. M. Büscher *et al.*, COSY Proposal #97 "Investigation of Neutral Scalar Mesons with ANKE" (2001); <http://www.fz-juelich.de/ikp/anke>